

Unified Performance Analysis of Reconfigurable Intelligent Surface Empowered Free Space Optical Communications

Vinay Kumar Chapala, *Graduate Student Member, IEEE* and
S. M. Zafaruddin, *Senior Member, IEEE*

Abstract

Reconfigurable intelligent surface (RIS) is an excellent use case for line-of-sight (LOS) based technologies such as free-space optical (FSO) communications. In this paper, we analyze the performance of RIS-empowered FSO (RISE-FSO) systems by unifying Fisher–Snedecor (\mathcal{F}), Gamma-Gamma (\mathcal{GG}), and Málaga (\mathcal{M}) distributions for atmospheric turbulence with zero-boresight pointing errors over deterministic as well as random path-loss in foggy conditions with heterodyne detection (HD) and intensity modulation/direct detection (IM/DD) methods. By deriving the probability density function (PDF) and cumulative distribution function (CDF) of the direct-link (DL) with the statistical effect of atmospheric turbulence, pointing errors and random fog, we develop exact expressions of PDF and CDF of the resultant channel for the RISE-FSO system. Using the derived statistical results, we present exact expressions of outage probability, average bit-error-rate (BER), ergodic capacity, and moments of signal-to-noise ratio (SNR) for both DL-FSO and RISE-FSO systems. We also develop an asymptotic analysis of the outage probability and average BER and derive the diversity order of the considered systems. We validate the analytical expressions using Monte-Carlo simulations and demonstrate the performance scaling of the FSO system with the number of RIS elements for various turbulence channels, detection techniques, and weather conditions.

Vinay Kumar Chapala (p20200110@pilani.bits-pilani.ac.in) and S. M. Zafaruddin (syed.zafaruddin@pilani.bits-pilani.ac.in) are with the Department of Electrical and Electronics Engineering, Birla Institute of Technology and Science, Pilani, Pilani-333031, Rajasthan, India.

This work was supported in part by the Science and Engineering Research Board (SERB), Department of Science and Technology (DST), Government of India, under Start-up Research Grant SRG/2019/002345.

Index Terms

Atmospheric turbulence, diversity order, free-space optical (FSO), Fox's H function, performance analysis, pointing errors, reconfigurable intelligent surface (RIS).

I. INTRODUCTION

Reconfigurable intelligent surface (RIS) is a promising technology to empower wireless systems by artificially controlling the characteristics of propagating signals in a desired direction [1]–[5]. Specifically, RISs are constructed by planar metasurfaces using a large number of reflection units adapted by integrated electronics to control the phase, amplitude and polarization of incident signals. The RIS is promising alternative to active relaying techniques without requiring complex processing at the relay to improve the performance of wireless systems. Free-space optical (FSO) communication is a potential technology to cater high data rate transmission with license free operation over a huge bandwidth in the optical spectrum [6]. Comparing with radio frequency (RF), FSO systems are immune to the electromagnetic interference and have been considered as a cost-effective solution for terrestrial backhaul/fronthaul wireless applications for 5G and beyond 5G networks [7], [8].

The FSO link is subjected to various channel impairments such as atmospheric turbulence, pointing errors, and other weather conditions. The atmospheric turbulence is the scintillation effect of light propagation in the atmosphere and introduces fading in the transmitted signal. In addition to the atmospheric turbulence, the range of FSO links is limited due to the higher signal attenuation, especially in the presence of fog and dust. Moreover, FSO is a line-of-sight (LOS) technology which may suffer significant performance degradation in the presence of pointing errors caused by the misalignment between the transmitter and the receiver. In this context, the deployment of FSO is not feasible for terrestrial applications due to the unavailability of direct link in the presence of obstructions creating dead-zones for wireless connectivity. The use of cooperative relaying has been extensively studied to mitigate the effect of channel impairments to improve the performance of FSO systems [9]–[12].

The advent of RIS opens an exciting research avenue to investigate and improve the performance of wireless systems for ubiquitous connectivity. Recently, the performance of RIS enabled wireless systems have been analyzed over radio-frequency (RF) transmissions [13]–[22], mixed RF-FSO [23]–[25], and FSO systems [26]–[30]. In [23], an RIS assisted dual-hop visible light communication (VLC)-RF system for an indoor scenario was proposed with VLC in the first

link and RIS in the second RF link. In [24], the authors considered a decode-and-forward (DF) relaying to mix an FSO link over Gamma-Gamma turbulence with pointing errors and RF link assisted with RIS over Rayleigh fading. In a similar setup, the mixed RF-FSO system was analyzed in [25] by considering an additional co-channel interference (CCI) in the RF link. The use of relaying in such systems decouples the performance analysis for FSO and RF such that the impact of RIS is present only in the RF link without the challenges of analyzing the RIS for FSO transmissions with complicated fading models. Recently, the authors in [26]–[30] employ RIS module for FSO systems. An overview of various design aspects of optical RIS for FSO comparing with RIS-assisted RF is presented [26]. The authors in [27] characterized the impact of the physical parameters of the RIS to model the geometric and misalignment losses due to the random movements of the RIS and the effect of building sway. In [28], multiple optical RISs are used to improve the outage probability of FSO system under the effect of pointing errors without considering the atmospheric turbulence. The authors in [29], [30] considered the Gamma-Gamma atmospheric turbulence with pointing errors to analyze the RIS based FSO system. However, the authors in [30] considered a simplified model by considering a single-element RIS to assist the FSO system. Moreover, the authors in [29] used the Gaussian distribution to analyze the RIS-assisted FSO system by employing the central limit theorem to approximate the distribution function of the end-to-end channel. It is desirable to provide an exact analysis of the FSO system with atmospheric turbulence combined with pointing errors and assisted by the RIS with multiple elements.

In the literature, there are several statistical models to characterize the atmospheric turbulence depending on the severity of turbulence, type of wave propagation, and mathematical tractability of the model. The Gamma-Gamma (\mathcal{GG}) is widely accepted for moderate-to-strong turbulence regime [31] whereas the generalized Málaga model (\mathcal{M}) can be used for all irradiance conditions in homogeneous and isotropic turbulence [32]. Recently, the Fisher–Snedecor \mathcal{F} -distribution model for the atmospheric turbulence is proposed for its mathematical tractability [33]. On the other hand, the zero-boresight model proposed by [34] is widely used in the literature to characterize the pointing errors in FSO systems. Traditionally, signal attenuation for FSO transmissions is assumed to be deterministic and quantified using a visibility range, for example, less attenuation in haze and light fog, and more loss of signal power in the dense fog [35]. However, recent measurement data confirm that the signal attenuation in the fog is not deterministic but follows a probabilistic model [36]. It should be noted that heterodyne detection (HD) and intensity

modulation/direct detection (IM/DD) are the two main modes of detection in FSO systems. Considering such a diversity operation, it is desirable to unify the FSO using different models of atmospheric turbulence with pointing errors, path loss, and detection modes.

In this paper, we analyze the performance of a RIS-empowered FSO (RISE-FSO) system by unifying \mathcal{F} , \mathcal{GG} , and \mathcal{M} distributions for atmospheric turbulence with zero-boresight pointing errors over deterministic as well as random path-loss in foggy conditions with HD and IM/DD modes of detection. It is emphasized that such a unification is not straight forward and it is not available even for the direct-link (DL) FSO systems. The major contributions of the proposed work are summarized as follows:

- We derive the probability density function (PDF) and cumulative distribution function (CDF) of the combined statistical effect of random fog with atmospheric turbulence and pointing errors of a DL-FSO system by unifying \mathcal{F} , \mathcal{GG} , and \mathcal{M} atmospheric turbulence models such that the traditional deterministic path loss model remains a particular case for a unified performance analysis.
- To analyze the RISE-FSO, we derive exact closed form expressions of PDF and CDF for the resultant channel realized by the sum of products (SOP) of fading coefficients considered to be independent but not identically distributed (i.n.i.d) according to the DL-FSO fading channel.
- Using the derived PDF and CDF, we analyze the performance of RISE-FSO system by developing exact closed-form expressions of the outage probability, average bit-error-rate (BER), ergodic capacity, and moments of signal-to-noise ratio (SNR) in terms of Fox's H function. For a comparison, we also develop exact analysis of the aforementioned performance metrics for the DL-FSO system, which is not available under the combined effect atmospheric turbulence, pointing errors, and random fog.
- We present asymptotic analysis for the outage probability and average BER in terms of simpler Gamma function in the high SNR regime. The asymptotic expressions are readily tractable and provide engineering insights for system design. As such, we derive diversity order using the outage probability and average BER depicting the impact of atmospheric turbulence, pointing errors, and foggy channel on system behavior, and the scaling of FSO performance with an increase in the number of RIS elements.
- We validate the derived analytical results using extensive Monte-Carlo simulations demonstrating the effectiveness of RISE-FSO in comparison with the DL-FSO system for various

atmospheric turbulence, detection techniques, and weather conditions.

A. Related Works

In this subsection, we summarize recent research works on RIS based RF systems. The authors in [13] analyzed outage probability, average bit-error-rate (BER) and bounds on capacity over Rayleigh fading RIS system. Considering the similar channel model, the authors in [14] presented exact and asymptotic analysis of ergodic capacity. In [15], performance of RIS-assisted and amplify-and-forward (AF) relaying wireless systems were compared for Rayleigh fading channel where the RIS assisted system was shown to outperform the corresponding relaying systems. In [16], for arbitrarily finite RIS elements, the authors offered closed-form estimates on the channel distribution over Rayleigh fading channels for dual-hop and transmit RIS-aided schemes. The authors used Rician fading to investigate the outage probability and ergodic capacity of a single-input single-output (SISO) RIS-assisted wireless communications system in [17]. The authors in [18], [19] approximated the average BER and ergodic capacity performance over Nakagami-m fading channels. An exact coverage analysis of RIS-enabled systems with Nakagami-m channels was presented in [20]. In [21], the authors derived exact expressions of the outage probability and ergodic capacity for a RIS-assisted system without pointing errors over generalized Fox's H fading channels. In [37], the authors considered α - μ fading model and analyzed the effective rate of RIS-assisted communications by simplifying the analysis using the mixture of Gaussian instead of considering the sum of cascaded α - μ distributed random variables. In [22], the authors analyzed a RIS-assisted millimeter-wave communication over the fluctuating two rays (FTR) fading model in terms of Fox's H function. Similarly, the authors in [38] extended the analysis for RIS-aided THz communications by deriving outage probability and ergodic capacity over FTR channel model combined with antenna misalignment and hardware impairments. The research on RIS assisted wireless systems is growing rapidly. To the best of authors' knowledge, an exact performance analysis on RIS empowered FSO system over generalized atmospheric turbulence with pointing errors is not publicly available.

B. Notations and Organizations

Main notations used in this paper are as follows: j denotes the imaginary number, $\mathbb{E}[\cdot]$ denotes the expectation operator, $\exp(\cdot)$ denotes the exponential function, while $\Gamma(a) = \int_0^\infty u^{a-1} e^{-u} du$

denotes the Gamma function. Finally, $G_{p,q}^{m,n} \left(x \left| \begin{array}{c} \{a_w\}_{w=1}^p \\ \{b_w\}_{w=1}^q \end{array} \right. \right)$ and $H_{p,q}^{m,n} \left(x \left| \begin{array}{c} \{(a_w, A_w)\}_{w=1}^p \\ \{(b_w, B_w)\}_{w=1}^q \end{array} \right. \right)$ denote Meijer-G and Fox's H functions respectively and a shortened notation $\{a_i\}_1^N = \{a_1, \dots, a_N\}$ to represent their coefficients.

The paper is organized as follows: system and channel models are summarized in section II followed by statistical distribution functions of DL-FSO and RISE-FSO systems in section III. Performance analysis through exact and asymptotic expressions is presented in section IV. The numerical and simulation results are discussed in section V. Finally, the paper concludes with section VI.

II. SYSTEM MODEL

We consider a single-aperture FSO system where the source S wishes to communicate with the destination D . We assume that there is no direct link between the source and destination. To facilitate transmissions for the RISE-FSO, we employ an N -element optical RIS such that a LOS exists from source to the RIS and RIS to the destination. Assuming perfect phase compensation at the RIS, the signal received at the destination through RIS is expressed as [29]

$$y = \sum_{i=1}^N h_i g_i s + \nu \quad (1)$$

where s is the transmitted signal with power P_T , h_i and g_i are channel fading coefficients between the source to the i -th RIS element and between the i -th RIS element to the destination, respectively, and ν is the additive Gaussian noise with variance σ_ν^2 . We denote by d the link distance between the source and destination, by d_1 the distance between the source and the RIS, and by d_2 the distance between the RIS and destination.

We consider that FSO links experience signal fading due to atmospheric turbulence, pointing errors, and foggy conditions such that the combined fading coefficient is denoted as $h_i = h_i^{(f)} h_i^{(t)} h_i^{(p)}$ and $g_i = g_i^{(f)} g_i^{(t)} g_i^{(p)}$, where superscripts (f) , (t) , and (p) denote the fog, atmospheric turbulence, and pointing errors, respectively. In what follows, we detail the modeling of the channel coefficient h_i . Note that we can model the channel coefficient g_i similar to h_i . However, we consider a general scenario considering fading coefficients $|h_i|$ and $|g_i|$ to be independent but non-identical distributed (i.ni.d).

To characterize the statistics of pointing errors $h_i^{(p)}$, we use the recently proposed model for optical RIS in [28], which is based on zero-boresight model [34]:

$$f_{h_i^{(p)}}(x) = \frac{\rho^2}{A_0^{\rho^2}} x^{\rho^2-1}, 0 \leq x \leq A_0, \quad (2)$$

where the term $A_0 = \text{erf}(v)^2$ denotes the fraction of collected power. Define $v = \sqrt{\pi/2} a_r/\omega_z$ with a_r as the aperture radius and ω_z as the beam width. We define the term $\rho^2 = \frac{\omega_{z\text{eq}}^2}{\xi}$ where $\omega_{z\text{eq}}$ is the equivalent beam width at the receiver. The use of $\xi = 4\sigma_s^2$ models the DL-FSO, where σ_s^2 is the variance of pointing errors displacement characterized by the horizontal sway and elevation [34], while $\xi = 4\sigma_1^2 d^2 + 16\sigma_2^2 d_2^2$ models the pointing errors for the RIS-FSO system, where σ_1 and σ_2 represent pointing error and RIS jitter angle standard deviation defined in [28].

For an unified performance analysis over a variety of turbulence conditions, we use the popular \mathcal{GG} [39], the generalized \mathcal{M} [32], and recently introduced \mathcal{F} - distribution [33] to model the atmospheric turbulence. We denote by $h_i^{(tp)} = h_i^{(t)} h_i^{(p)}$ the combined effect of atmospheric turbulence and pointing errors. We represent the PDF of FSO link with \mathcal{GG} fading and pointing errors as given in [40]:

$$f_{h_i^{(tp)}}^{\text{GP}}(x) = \frac{\alpha_G \beta_G \rho^2}{A_0 \Gamma(\alpha_G) \Gamma(\beta_G)} G_{1,3}^{3,0} \left(\frac{\alpha_G \beta_G h}{A_0} \left| \begin{array}{c} \rho^2 \\ \rho^2 - 1, \alpha_G - 1, \beta_G - 1 \end{array} \right. \right) \quad (3)$$

where the fading parameters α_G and β_G are defined in [39]. Similarly, the PDF of \mathcal{M} -distributed turbulence combined with pointing errors is given as [10]:

$$f_{h_i^{(tp)}}^{\text{MP}}(x) = \frac{\rho^2 A_{\text{mg}}}{2x} \sum_{m=1}^{\beta_M} b_m G_{1,3}^{3,0} \left(\frac{\alpha_M \beta_M}{g \beta_M + \Omega'} \frac{x}{A_0} \left| \begin{array}{c} \rho^2 + 1 \\ \rho^2, \alpha_M, m \end{array} \right. \right), \quad (4)$$

where the parameters α_M , β_M , A_{mg} , b_m , and Ω' are given in [32]. Finally, the PDF of FSO channel experiencing \mathcal{F} -turbulence in the presence of pointing error impairments is given as [33]:

$$f_{h_i^{(tp)}}^{\text{FP}}(x) = \frac{\alpha_F \rho^2 G_{2,2}^{2,1} \left[\frac{\alpha_F}{(\beta_F - 1) A_0} x \left| \begin{array}{c} -\beta_F, \rho^2 \\ \beta_F - 1, \rho^2 - 1 \end{array} \right. \right]}{(\beta_F - 1) A_0 \Gamma(\alpha_F) \Gamma(\beta_F)} \quad (5)$$

where the fading parameters α_F and β_F are listed in [41].

The channel coefficient $h_i^{(f)}$ models the path gain of signal transmission over the FSO link. Generally, $h_i^{(f)}$ is a deterministic quantity obtained from Beer-Lambert's Law $h_i^{(f)} = e^{-\tau d}$ where d is the link distance (in km) and τ is the atmospheric attenuation factor which depends on the wavelength and visibility range [35]. The atmospheric attenuation is defined as

$\tau = \frac{3.19}{V} \left(\frac{\lambda}{550 \text{ nm}} \right)^{-q_v}$ where V is the visibility (in km), λ is operating wavelength (in nm), and q_v is the size distribution of the scattering particles given by

$$q_v = \begin{cases} 0, & \text{for fog } V < 500 \text{ m} \\ V - 0.5, & \text{for mist } 500 \text{ m} < V < 1 \text{ km} \\ 0.16V + 0.34, & \text{for haze } 1 \text{ km} < V < 6 \text{ km}. \end{cases} \quad (6)$$

However, recent studies [36], [42] show that the path gain in foggy conditions exhibit randomness modeled with the following PDF

$$f_{h_i^{(f)}}(x) = \frac{v^k}{\Gamma(k)} \left[\ln \left(\frac{1}{x} \right) \right]^{k-1} x^{v-1}, \quad (7)$$

where $0 < x \leq 1$, $v = 4.343/d\beta^{\text{fog}}$, $k > 0$ is the shape parameter, and $\beta^{\text{fog}} > 0$ is the scale parameter.

We also consider the DL-FSO system by considering the existence of direct link between the source and destination, as a means to compare with the RISE-FSO system:

$$y = h^{\text{DL}} s + \nu \quad (8)$$

where h^{DL} denotes the channel coefficient of the direct link. It should be noted that the performance of DL-FSO system with various atmospheric turbulence and pointing errors has been extensively studied in the literature. However, an exact analysis for the DL-FSO system with the effect of random fog is not available. In [43], we have developed asymptotic analysis by considering exponentiated Weibul model for atmospheric turbulence with pointing errors and random fog.

III. STATISTICAL RESULTS

In this section, we develop the PDF and CDF of the resultant channel $h = \sum_{i=1}^N h_i g_i$ of RISE-FSO system. First, we find density and distribution functions of the combined channel $h_i = h_i^{(f)} h_i^{(t)} h_i^{(p)}$ by unifying the PDF of various atmospheric turbulence with pointing errors as given in (3), (4), and (5). Next, we develop statistical results of $Z_i = h_i g_i$ using Melin's transform. Finally, we use the MGF of Z_i to get the PDF and CDF of $Z = \sum_{i=1}^N Z_i$.

Proposition 1. *An unified PDF for the combined effect of atmospheric turbulence and pointing errors is given as*

$$f_{h_i^{(tp)}}(x) = \psi x^{\phi-1} \sum_{l=1}^P \zeta_l G_{p,q}^{m,n} \left(C_l x \left| \begin{array}{l} \{a_{l,w}\}_{w=1}^p \\ \{b_{l,w}\}_{w=1}^q \end{array} \right. \right) \quad (9)$$

TABLE I
PARAMETERS OF THE UNIFIED PDF (PROPOSITION 1)

Turbulence Model	Unified parameters
\mathcal{GG}	$\psi = \frac{\alpha_G \beta_G \rho^2}{A_0 \Gamma(\alpha_G) \Gamma(\beta_G)}, \phi = 1, P = 1, \zeta_1 = 1, C_1 = \frac{\alpha_G \beta_G}{A_0},$ $\{m, n, p, q\} = \{3, 0, 1, 3\}, a = \{\rho^2\}, b = \{\rho^2 - 1, \alpha_G - 1, \beta_G - 1\}$
\mathcal{M}	$\psi = \frac{\rho^2 A_M \rho}{2}, \phi = 0, P = \beta_M, \zeta_1 = b_l, C_1 = \frac{\alpha_M \beta_M}{(g \beta_M + \Omega') A_0},$ $\{m, n, p, q\} = \{3, 0, 1, 3\}, a = \{\rho^2 + 1\}, b = \{\rho^2, \alpha_M, l\}$
\mathcal{F}	$\psi = \frac{\alpha_F \rho^2}{(\beta_F - 1) h_l A_0 \Gamma(\alpha_F) \Gamma(\beta_F)}, \phi = 1, P = 1, \zeta_1 = 1, C_1 = \frac{\alpha_F}{(\beta_F - 1) h_l A_0},$ $\{m, n, p, q\} = \{2, 1, 2, 2\}, a = \{-\beta_F, \rho^2\}, b = \{\alpha_F - 1, \rho^2 - 1\}$

where parameters in (9) define specific atmospheric turbulence model, as given in Table I.

Proof: We use (9) as a general fading model and derive the parameters of specific models using (3), (4), and (5), as depicted in Table I. ■

It is straightforward to use (9) and find the PDF of combined channel $h_i = h_i^{(tp)} h_i^{(f)}$ if the channel gain $h_i^{(f)}$ is considered to be deterministic. In the following Theorem, we develop a novel PDF considering the channel gain $h_i^{(f)}$ to be distributed according to (7) in the presence of fog.

Theorem 1. *If k and v are the parameters of the foggy channel and Table I depicts the parameters for atmospheric turbulence and pointing errors, then the PDF and CDF of the combined fading channel with atmospheric turbulence, pointing errors, and random fog are given by*

$$f_{h_i}(x) = \psi v^k \sum_{l=1}^P \zeta_l x^{\phi-1} G_{p+k, q+k}^{m+k, n} \left[C_l x \left| \begin{array}{c} \{a_{l,w}\}_{w=1}^p, \{v - \phi + 1\}_1^k \\ \{b_{l,w}\}_{w=1}^m, \{v - \phi\}_1^k, \{b_{l,w}\}_{w=m+1}^q \end{array} \right. \right] \quad (10)$$

$$F_{h_i}(x) = \psi v^k \sum_{l=1}^P \zeta_l x^\phi G_{p+k+1, q+k+1}^{m+k, n+1} \left[C_l x \left| \begin{array}{c} \{a_{l,w}\}_{w=1}^n, \{1 - \phi\}, \{a_{l,w}\}_{w=n+1}^p, \{v - \phi + 1\}_1^k \\ \{b_{l,w}\}_{w=1}^m, \{v - \phi\}_1^k, \{b_{l,w}\}_{w=m+1}^q, \{-\phi\} \end{array} \right. \right] \quad (11)$$

Proof: See Appendix A. ■

Since the underlying PDFs in (9) and (10) have similar structure, the unified performance analysis presented in this paper is applicable for both deterministic and random path loss model. As such the PDF represented in (10) can be reduced to (9) for the deterministic path gain by substituting $k = 0$ and limiting the Meijer's G argument upto p and q terms. We also verify the

validity of the derived PDF in (10) by considering \mathcal{F} turbulence. Thus, we use parameters from Table I for the \mathcal{F} -distribution and apply the identity [44, 07.34.21.0009.01] to get

$$\begin{aligned} \int_0^\infty f_{h_i}(x) dx &= \frac{\alpha_F \rho^2 v^k}{(\beta_F - 1) A_0 \Gamma(\alpha_F) \Gamma(\beta_F)} \int_0^\infty G_{k+2, k+2}^{k+2, 1} \left[\frac{\alpha_F}{(\beta_F - 1) A_0} x \left| \begin{array}{c} -\beta_F, \rho^2, \{v\}_1^k \\ \alpha_F - 1, \rho^2 - 1, \{v - 1\}_1^k \end{array} \right. \right] dx \\ &= \frac{\alpha_F \rho^2 v^k}{(\beta_F - 1) A_0 \Gamma(\alpha_F) \Gamma(\beta_F)} \frac{\Gamma(\alpha_F) \Gamma(\rho^2) (\Gamma(v))^k \Gamma(\beta_F) (\beta_F - 1) A_0}{\Gamma(1 + \rho^2) (\Gamma(1 + v))^k} \frac{1}{\alpha_F} = 1 \end{aligned} \quad (12)$$

To facilitate performance analysis for the RISE-FSO, the distribution function of $\sum_{i=1}^N h_i g_i$ is required. Considering L reflecting paths in each RIS element, we derive the PDF and CDF of the generalized system $Z = \sum_{i=1}^N Z_i$, where $Z_i = \prod_{j=1}^L h_{i,j}$ and $h_{i,j}, j = 1, 2, \dots, L$ are i.n.i.d random variable distributed according to (10). Note that we can use results of Theorem 1 to analyze the performance DL-FSO system.

Proposition 2. *If k and v are the parameters of the foggy channel and Table I depicts the parameters for atmospheric turbulence and pointing errors, then the PDF and CDF, and MGF of product of L independent but non-identical (i.n.i.d) random variables $Z_i = \prod_{j=1}^L h_{i,j}$ are given by*

$$f_{Z_i}(x) = \frac{1}{x} \sum_{l_1, \dots, l_L=0}^P \prod_{j=1}^L \psi_j v_j^{k_j} \zeta_{l_j} \left(C_{l_j} \right)^{-\phi_j} G_{pL + \sum_{j=1}^L k_j, qL + \sum_{j=1}^L k_j}^{mL + \sum_{j=1}^L k_j, nL} \left[x \prod_{j=1}^L C_{l_j} \left| \begin{array}{c} V_1, V_2 \\ V_3 \end{array} \right. \right] \quad (13)$$

$$F_{Z_i}(x) = \sum_{l_1, \dots, l_L=0}^P \prod_{j=1}^L \psi_j v_j^{k_j} \zeta_{l_j} \left(C_{l_j} \right)^{-\phi_j} G_{pL + \sum_{j=1}^L k_j + 1, qL + \sum_{j=1}^L k_j + 1}^{mL + \sum_{j=1}^L k_j, nL + 1} \left[x \prod_{j=1}^L C_{l_j} \left| \begin{array}{c} V_1, \{1\}, V_2 \\ V_3, \{0\} \end{array} \right. \right] \quad (14)$$

$$M_{Z_i}(s) = \sum_{l_1, \dots, l_L=0}^P \prod_{j=1}^L \psi_j v_j^{k_j} \zeta_{l_j} \left(C_{l_j} \right)^{-\phi_j} G_{pL + \sum_{j=2}^L k_j + 1, qL + \sum_{j=1}^L k_j}^{mL + \sum_{j=1}^L k_j, nL + 1} \left[\frac{1}{s} \prod_{j=1}^L C_{l_j} \left| \begin{array}{c} V_1, \{1\}, V_2 \\ V_3 \end{array} \right. \right] \quad (15)$$

where $V_1 = \{\{\phi_j + a_{l_j, w}\}_{j=1}^L\}_{w=1}^n$, $V_2 = \{\{\phi_j + a_{l_j, w}\}_{j=1}^L\}_{w=n+1}^p$, $\{\{v_j + 1\}_1^{k_j}\}_{j=1}^L$ and $V_3 = \{\{\phi_j + b_{l_j, w}\}_{j=1}^L\}_{w=1}^m$, $\{\{v_j\}_1^{k_j}\}_{j=1}^L$, $\{\{\phi_j + b_{l_j, w}\}_{j=1}^L\}_{w=m+1}^q$.

Proof: See Appendix B. ■

Theorem 2. *If k and v are the parameters of the foggy channel and Table I depicts the parameters for atmospheric turbulence and pointing errors, then the PDF and CDF of $Z = \sum_{i=1}^N Z_i$ are*

$$f_Z(x) = \frac{1}{x} \sum_{l_{1,1}, \dots, l_{1,L}=0}^P \cdots \sum_{l_{N,1}, \dots, l_{N,L}=0}^P \prod_{i=1}^N \prod_{j=1}^L \psi_{i,j} v_{i,j}^{k_{i,j}} \zeta_{l_{i,j}} \left(C_{l_{i,j}} \right)^{-\phi_{i,j}}$$

$$H_{0,1:pL+\sum_{j=1}^L k_{1,j}+1, qL+\sum_{j=1}^L k_{1,j}; \dots; mL+\sum_{j=1}^L k_{N,j}, nL+1}^{0,0:mL+\sum_{j=1}^L k_{1,j}, nL+1; \dots; mL+\sum_{j=1}^L k_{N,j}, nL+1} \left[\begin{array}{c} x \prod_{j=1}^L C_{l_{i,j}} \\ \vdots \\ x \prod_{j=1}^L C_{l_{i,j}} \end{array} \middle| \begin{array}{l} - : V_1 \\ (1; 1, \dots, 1) : V_2 \end{array} \right] \quad (16)$$

$$F_Z(x) = \sum_{l_{1,1}, \dots, l_{1,L}=0}^P \cdots \sum_{l_{N,1}, \dots, l_{N,L}=0}^P \prod_{i=1}^N \prod_{j=1}^L \psi_{i,j} v_{i,j}^{k_{i,j}} \zeta_{l_{i,j}} \left(C_{l_{i,j}} \right)^{-\phi_{i,j}}$$

$$H_{0,1:pL+\sum_{j=1}^L k_{1,j}+1, qL+\sum_{j=1}^L k_{1,j}; \dots; mL+\sum_{j=1}^L k_{N,j}, nL+1}^{0,0:mL+\sum_{j=1}^L k_{1,j}, nL+1; \dots; mL+\sum_{j=1}^L k_{N,j}, nL+1} \left[\begin{array}{c} x \prod_{j=1}^L C_{l_{i,j}} \\ \vdots \\ x \prod_{j=1}^L C_{l_{i,j}} \end{array} \middle| \begin{array}{l} - : V_1 \\ (0; 1, \dots, 1) : V_2 \end{array} \right] \quad (17)$$

where $V_1 = \{ \{ \{ (\phi_{i,j} + a_{l_{i,j},w}, 1) \}_{j=1}^L \}_{w=1}^n, (1, 1), \{ \{ (\phi_{i,j} + a_{l_{i,j},w}, 1) \}_{j=1}^L \}_{w=n+1}^p, \{ \{ (v_{i,j} + 1, 1) \}_1^{k_{i,j}} \}_{j=1}^L \}_{i=1}^N$
and $V_2 = \{ \{ \{ (\phi_{i,j} + b_{l_{i,j},w}, 1) \}_{j=1}^L \}_{w=1}^m, \{ \{ (v_{i,j}, 1) \}_1^{k_{i,j}} \}_{j=1}^L, \{ \{ (\phi_{i,j} + b_{l_{i,j},w}, 1) \}_{j=1}^L \}_{w=m+1}^q, \{ \{ (v_{i,j}, 1) \}_1^{k_{i,j}} \}_{j=1}^L \}_{i=1}^N$.

Proof: See Appendix C. ■

We can validate the derived PDF in (16) by $\int_0^\infty f_Z(z) dz = 1$. Using the parameters of \mathcal{F} -distributed atmospheric turbulence from Table I in (16), we use the definition of Fox's H function and interchange the order of integration to solve the inner integral using the final value theorem:

$\int_0^\infty x^{-1-\sum_{i=1}^N x_i} dz = \lim_{s \rightarrow 0} (\frac{1}{s})^{-\sum_{i=1}^N x_i} \Gamma(-\sum_{i=1}^N x_i)$. Thus, we get

$$\int_0^\infty f_Z(z) dz = \lim_{s \rightarrow 0} \prod_{i=1}^N \prod_{j=1}^L \frac{\rho_{i,j}^2 v_{i,j}^{k_{i,j}}}{\Gamma(\alpha_F(i, j)) \Gamma(\beta_F(i, j))} H_{0,0:2L+\sum_{j=1}^L k_{1,j}; \dots; L+1, 2L+\sum_{j=1}^L k_{N,j}}^{0,0:L+1, 2L+\sum_{j=1}^L k_{1,j}; \dots; L+1, 2L+\sum_{j=1}^L k_{N,j}}$$

$$\left[\begin{array}{c} s \prod_{j=1}^L \frac{(\beta_F(i, j) - 1) h_i A_0}{\alpha_F(i, j)} \\ \vdots \\ s \prod_{j=1}^L \frac{(\beta_F(i, j) - 1) h_i A_0}{\alpha_F(i, j)} \end{array} \middle| \begin{array}{l} - : \{ \{ (1 - \alpha_F(i, j), 1) \}_{j=1}^L, \{ (1 - \rho_{i,j}^2, 1) \}_{j=1}^L, \{ \{ (1 - v_{i,j}, 1) \}_1^{k_{i,j}} \}_{j=1}^L \}_{i=1}^N \\ - : \{ (0, 1), \{ (\beta_F(i, j), 1) \}_{j=1}^L, \{ (-\rho_{i,j}^2, 1) \}_{j=1}^L, \{ \{ (-v_{i,j}, 1) \}_1^{k_{i,j}} \}_{j=1}^L \}_{i=1}^N \end{array} \right] \quad (18)$$

Finally, we use [45] and apply standard Mathematical procedures in (18) to validate the PDF:

$$\int_0^\infty f_Z(z) dz = \prod_{i=1}^N \prod_{j=1}^L \frac{\rho_{i,j}^2 v_{i,j}^{k_{i,j}}}{\Gamma(\alpha_F(i,j)) \Gamma(\beta_F(i,j))} \frac{\Gamma(\beta_F(i,j)) \Gamma(\alpha_F(i,j)) \Gamma(\rho_{i,j}^2) \left(\Gamma(v_{i,j}) \right)^{k_{i,j}}}{\Gamma(1 + \rho_{i,j}^2) \left(\Gamma(1 + v_{i,j}) \right)^{k_{i,j}}} = 1 \quad (19)$$

In what follows, we analyze the performance of RISE-FSO and DL-FSO systems using the statistical results of Theorem 1 and Theorem 2, respectively.

IV. PERFORMANCE ANALYSIS

In this section, we analyze the performance of the RISE-FSO by a simple customization of Theorem 2 with $L = 2$, $z_{i,1} = h_i$, and $z_{i,2} = g_i$, which corresponds to the RISE-FSO system model in (1). Thus, we denote the resultant by $h = \sum_{i=1}^N h_i g_i$. Finally, we introduce the third unification of performance evaluation with HD ($t = 1$) and IM/DD ($t = 2$) detection modes by defining SNR of the system as $\gamma = \gamma_0 h^t$, where $\gamma_0 = \frac{P_T^t}{\sigma_v^2}$. A straightforward transformation of random variable in (16) and (17) leads to the PDF $f_\gamma(\gamma)$ and the CDF $F_\gamma(\gamma)$ of SNR as

$$f_\gamma(\gamma) = \frac{1}{t \gamma_0^{\frac{1}{t}} \gamma^{1 - \frac{1}{t}}} f_Z \left(\left(\frac{\gamma}{\gamma_0} \right)^{1/t} \right) \quad (20)$$

$$F_\gamma(\gamma) = F_Z \left(\left(\frac{\gamma}{\gamma_0} \right)^{1/t} \right) \quad (21)$$

Similarly, we use (10) and (11) to express the PDF and CDF of SNR for the DL-FSO as

$$f_\gamma^{\text{DL}}(\gamma) = \frac{1}{t \gamma_0^{\frac{1}{t}} \gamma^{1 - \frac{1}{t}}} f_{h_i} \left(\left(\frac{\gamma}{\gamma_0} \right)^{1/t} \right), \quad F_\gamma^{\text{DL}}(\gamma) = F_{h_i} \left(\left(\frac{\gamma}{\gamma_0} \right)^{1/t} \right) \quad (22)$$

A. Outage Probability

Outage probability is a performance metric to characterize the impact of fading in a communication system. Mathematically, it can be defined as the probability of SNR falling below a threshold value γ_{th} i.e., $P_{\text{out}} = Pr(\gamma \leq \gamma_{\text{th}})$.

Lemma 1. *We present the following results of outage probability for the RISE-FSO system:*

(a) *An exact expression for the outage probability is given as $P_{\text{out}} = F_\gamma(\gamma_{\text{th}})$.*

TABLE II
DIVERSITY ORDER OF RISE-FSO

Turbulence Model	G_{out} with $\kappa = 0$ and G_{BER} with $\kappa = 1$
\mathcal{GG}	$\sum_{i=1}^N \min\left\{\frac{\alpha_G(i,1)-\kappa}{t}, \frac{\beta_G(i,1)-\kappa}{t}, \frac{\rho_{i,1}^2-\kappa}{t}, \frac{v_{i,1}-\kappa}{t}, \frac{\alpha_G(i,2)-\kappa}{t}, \frac{\beta_G(i,2)-\kappa}{t}, \frac{\rho_{i,2}^2-\kappa}{t}, \frac{v_{i,2}-\kappa}{t}\right\}$
\mathcal{M}	$\sum_{i=1}^N \min\left\{\frac{\alpha_M(i,1)-\kappa}{t}, \frac{\beta_M(i,1)-\kappa}{t}, \frac{\rho_{i,1}^2-\kappa}{t}, \frac{v_{i,1}-\kappa}{t}, \frac{\alpha_M(i,2)-\kappa}{t}, \frac{\beta_M(i,2)-\kappa}{t}, \frac{\rho_{i,2}^2-\kappa}{t}, \frac{v_{i,2}-\kappa}{t}\right\}$
\mathcal{F}	$\sum_{i=1}^N \min\left\{\frac{\alpha_F(i,1)-\kappa}{t}, \frac{\rho_{i,1}^2-\kappa}{t}, \frac{v_{i,1}-\kappa}{t}, \frac{\alpha_F(i,2)-\kappa}{t}, \frac{\rho_{i,2}^2-\kappa}{t}, \frac{v_{i,2}-\kappa}{t}\right\}$

(b) Asymptotically at a high SNR, the outage probability is

$$P_{\text{out}}^{\infty} \approx \sum_{l_{1,1}, l_{1,2}=0}^P \cdots \sum_{l_{N,1}, l_{N,2}=0}^P \prod_{i=1}^N \prod_{j=1}^2 \psi_{i,j} v_{i,j}^{k_{i,j}} \zeta_{l_{i,j}} \left(C_{l_{i,j}}\right)^{-\phi_{i,j}} \left(\frac{\gamma_{\text{th}}}{\gamma_0}\right)^{p_i/t} \left(\prod_{j=1}^2 C_{l_{i,j}}\right)^{p_i} \frac{1}{\Gamma(1+\sum_{i=1}^N p_i)}$$

$$\prod_{i=1}^N \frac{\prod_{j=1}^2 \prod_{w=1, p_i \neq \phi_{i,j} + b_{l_{i,j}, w}}^m \Gamma(\phi_{i,j} + b_{l_{i,j}, w} - p_i) \prod_{j=1}^2 \prod_{w=1, p_i \neq v_{i,j}}^{k_{i,j}} \left(\Gamma(v_{i,j} - p_i)\right)^{k_{i,j}} \prod_{j=1}^2 \prod_{w=1}^n \Gamma(1 - \phi_{i,j} - a_{l_{i,j}, w} + p_i) \Gamma(p_i)}{\prod_{j=1}^2 \prod_{w=n+1}^p \Gamma(\phi_{i,j} + a_{l_{i,j}, w} - p_i) \prod_{j=1}^2 \left(\Gamma(v_{i,j} + 1 - p_i)\right)^{k_{i,j}} \prod_{j=1}^2 \prod_{w=m+1}^q \Gamma(1 - \phi_{i,j} - b_{l_{i,j}, w} + p_i)} \quad (23)$$

where $p_i = \min\{\{\phi_{i,j} + b_{l_{i,j}, w}\}_{w=1}^m, v_{i,j}\}_{j=1}^2$.

(c) The diversity order is given as $G_{\text{out}} = \sum_{i=1}^N \min\left\{\frac{\phi_{i,1} + b_{l_{i,1}, w}}{t}\right\}_{w=1}^m, \frac{v_{i,1}}{t}, \left\{\frac{\phi_{i,2} + b_{l_{i,2}, w}}{t}\right\}_{w=1}^m, \frac{v_{i,2}}{t}\right\}$.

Proof: (a) can be obtained using the direct definition of the outage probability. To prove (b), we use [45] to derive the outage probability asymptotically at a high SNR $\gamma_0 \rightarrow \infty$ in terms of Gamma function. To prove (c), we express (23) as $P_{\text{out}}^{\infty} \propto \gamma_0^{-G_{\text{out}}}$ in order to get the outage-diversity order G_{out} of the system. ■

We present Table II with $\kappa = 0$ for the diversity order of RISE-FSO system for three turbulence models and both the HD and IM/DD detection modes. It can be seen that the outage performance of the RISE-FSO improves with an increase in the number of RIS elements.

For the DL-FSO system, an exact expression of the outage probability can be obtained using the CDF in (22) and (11) as $P_{\text{out}}^{\text{DL}} = F_{\gamma}^{\text{DL}}(\gamma_{\text{th}})$. We use the asymptotic representation of the Meijer's G function [44, 07.34.06.0005.01] on the derived $P_{\text{out}}^{\text{DL}}$ to express the outage probability in the high SNR regime $\gamma_0 \rightarrow \infty$:

$$P_{\text{out}}^{\infty, \text{DL}} \approx \psi v^k \sum_{l=1}^P \zeta_l C_l^{\gamma-\phi} \left[\sum_{i=1}^m \frac{\prod_{w=1, w \neq i}^m \Gamma(b_{l,w} - b_{l,i}) (\Gamma(v - \phi - b_{l,i}))^k \prod_{w=1}^n \Gamma(1 - a_{l,w} + b_{l,i}) \Gamma(\phi + b_{l,i})}{\prod_{w=n+1}^p \Gamma(a_{l,w} - b_{l,i}) (\Gamma(v + 1 - \phi - b_{l,i}))^k \prod_{w=m+1}^q \Gamma(1 - b_{l,w} + b_{l,i}) \Gamma(1 + \phi + b_{l,i})} \right. \\ \left. \left(C_l^{\phi + b_{l,i}} \left(\frac{\gamma_{\text{th}}}{\gamma_0}\right)^{(\phi + b_{l,i})/t} \right) + k \frac{\prod_{w=1}^m \Gamma(\phi + b_{l,w} - v) \prod_{w=1}^n \Gamma(1 - \phi - a_{l,w} + v) \Gamma(v)}{\prod_{w=n+1}^p \Gamma(\phi + a_{l,w} - v) \prod_{w=m+1}^q \Gamma(1 - \phi - b_{l,w} + v) \Gamma(1 + v)} \left(C_l^v \left(\frac{\gamma_{\text{th}}}{\gamma_0}\right)^{v/t} \right) \right] \quad (24)$$

We can express $P_{\text{out}}^{\infty, \text{DL}} \propto \gamma_0^{-G_{\text{out}}^{\text{DL}}}$ in (24) to get the diversity order of the DL-FSO system as $G_{\text{out}}^{\text{DL}} = \min(\{\frac{\phi + b_{l,i}}{t}\}_{l=1, i=1}^{l=P, i=m}, \frac{v}{t})$. Using Table I, the diversity order for \mathcal{F} , \mathcal{GG} , and \mathcal{M}

turbulence with pointing errors and random fog parameter are respectively, $\min\{\frac{\alpha_F}{t}, \frac{\rho^2}{t}, \frac{v}{t}\}$, $\min\{\frac{\rho^2}{t}, \frac{\alpha_G}{t}, \frac{\beta_G}{t}, \frac{v}{t}\}$, and $\min\{\frac{\rho^2}{t}, \frac{\alpha_M}{t}, \frac{\beta_M}{t}, \frac{v}{t}\}$. This is consistent with previous results of diversity order for DL-FSO systems with atmospheric turbulence and pointing errors with deterministic path loss (see [10] [11] [41], and references therein).

B. Average BER

Average BER is used to quantify the reliability of data transmissions. The average BER using the CDF of SNR is given as [46]

$$\bar{P}_e = \frac{q^p}{2\Gamma(p)} \int_0^\infty \gamma^{p-1} e^{-q\gamma} F_\gamma(\gamma) d\gamma \quad (25)$$

where p and q are modulation specific parameters. Specifically, for coherent binary FSK (CBFSK), $p = q = 0.5$, coherent binary PSK (CBPSK), $p = 0.5$ and $q = 1$, non-coherent binary FSK (NBFSK), $p = 1$ and $q = 0.5$, differential binary PSK (DBPSK), $p = 1$ and $q = 1$. For M-ary pulse position modulation (M-PPM), $p = 0.5, q = M \log_2(M)/16$, while for M-ary pulse amplitude modulation (M-PAM), $p = 0.5$ and $q = \log_2(M)/8(M-1)^2$.

Lemma 2. *We present the following results of the average BER for the RISE-FSO system:*

(a) *An exact expression for the average BER is given by*

$$\bar{P}_e = \left(\frac{1}{2\Gamma(p)} \right) \sum_{l_{1,1}, l_{1,2}=0}^P \cdots \sum_{l_{N,1}, l_{N,2}=0}^P \prod_{i=1}^N \prod_{j=1}^2 \psi_{i,j} v_{i,j}^{k_{i,j}} \zeta_{l_{i,j}} \left(C_{l_{i,j}} \right)^{-\phi_{i,j}} \quad (26)$$

$$H_{1,1:2m+k_{1,1}+k_{1,2}, 2n+1; \dots; 2m+k_{N,1}+k_{N,2}, 2n+1}^{0,1} \left[\begin{array}{c} \left(\frac{1}{q\gamma_0} \right)^{1/t} \prod_{j=1}^2 C_{l_{i,j}} \\ \cdot \\ \cdot \\ \left(\frac{1}{q\gamma_0} \right)^{1/t} \prod_{j=1}^2 C_{l_{i,j}} \end{array} \middle| \begin{array}{l} (1-p, \frac{1}{t}, \dots, \frac{1}{t}) : V_1 \\ (0; 1, \dots, 1) : V_2 \end{array} \right]$$

where $V_1 = \{ \{(\phi_{i,1} + a_{l_{i,1},w}, 1)\}_{w=1}^n, \{(\phi_{i,2} + a_{l_{i,2},w}, 1)\}_{w=1}^n, (1, 1), \{(\phi_{i,1} + a_{l_{i,1},w}, 1)\}_{w=n+1}^p, \{(\phi_{i,2} + a_{l_{i,2},w}, 1)\}_{w=n+1}^p, \{(v_{i,1} + 1, 1)\}_1^{k_{i,1}}, \{(v_{i,2} + 1, 1)\}_1^{k_{i,2}} \}_{i=1}^N$ and $V_2 = \{ \{(\phi_{i,1} + b_{l_{i,1},w}, 1)\}_{w=1}^m, \{(\phi_{i,2} + b_{l_{i,2},w}, 1)\}_{w=1}^m, \{(v_{i,1}, 1)\}_1^{k_{i,1}}, \{(v_{i,2}, 1)\}_1^{k_{i,2}}, \{(\phi_{i,1} + b_{l_{i,1},w}, 1)\}_{w=m+1}^q, \{(\phi_{i,2} + b_{l_{i,2},w}, 1)\}_{w=m+1}^q \}_{i=1}^N$.

(b) *Asymptotically at high SNR $\gamma_0 \rightarrow \infty$, the average BER can be expressed as*

$$\bar{P}_e^\infty \approx \sum_{l_{1,1}, l_{1,2}=0}^P \cdots \sum_{l_{N,1}, l_{N,2}=0}^P \prod_{i=1}^N \prod_{j=1}^2 \psi_{i,j} v_{i,j}^{k_{i,j}} \zeta_{l_{i,j}} \left(C_{l_{i,j}} \right)^{N+p_i-1-\phi_{i,j}} \left(\frac{1}{q\gamma_0} \right)^{\frac{p_i-1}{t}} \left(\frac{1}{q} \right)^{N/t} \frac{\Gamma(p+\frac{1}{t} \sum_{i=1}^N p_i)}{\Gamma(1+\sum_{i=1}^N p_i)}$$

$$\prod_{i=1}^N \frac{\prod_{j=1}^2 \prod_{w=1, p_i \neq \phi_{i,j} + b_{l_{i,j},w}}^m \Gamma(\phi_{i,j} + b_{l_{i,j},w} - p_i) \prod_{j=1}^2 \prod_{w=1, p_i \neq v_{i,j}}^{k_{i,j}} \left(\Gamma(v_{i,j} - p_i) \right)^{k_{i,j}} \prod_{j=1}^2 \prod_{w=1}^n \Gamma(1 - \phi_{i,j} - a_{l_{i,j},w} + p_i) \Gamma(p_i)}{\prod_{j=1}^2 \prod_{w=n+1}^p \Gamma(\phi_{i,j} + a_{l_{i,j},w} - p_i) \prod_{j=1}^2 \left(\Gamma(v_{i,j} + 1 - p_i) \right)^{k_{i,j}} \prod_{j=1}^2 \prod_{w=m+1}^q \Gamma(1 - \phi_{i,j} - b_{l_{i,j},w} + p_i)} \quad (27)$$

where $p_i = \min\{\{\phi_{i,1} + b_{l_{i,1},w}\}_{w=1}^m, v_{i,1}, \{\phi_{i,2} + b_{l_{i,2},w}\}_{w=1}^m, v_{i,2}\}$.

(c) The diversity order using the average BER is $G_{\text{BER}} = \sum_{i=1}^N \min\{\{\frac{\phi_{i,j} + b_{l_{i,j},w-1}}{t}\}_{w=1}^m, \frac{v_{i,j}-1}{t}\}_{j=1}^2$.

Proof: To prove (a), we substitute the CDF of RISE-FSO system of (21) (which requires (17)) in (25), use the definition of multivariate Fox-H function, and interchange the order of integration to get

$$\begin{aligned} \bar{P}_e = & \left(\frac{q^p}{2\Gamma(p)} \right) \sum_{l_{1,1}, l_{1,2}=0}^P \cdots \sum_{l_{N,1}, l_{N,2}=0}^P \prod_{i=1}^N \prod_{j=1}^2 \psi_{i,j} v_{i,j}^{k_{i,j}} \zeta_{l_{i,j}} \left(C_{l_{i,j}} \right)^{-\phi_{i,j}} \left(\left(\frac{1}{2\pi j} \right)^N \int_{\mathcal{L}_i} \left(\left(\frac{1}{\gamma_0} \right)^{1/t} \prod_{j=1}^2 C_{l_{i,j}} \right)^{x_i} \right. \\ & \left[\frac{\prod_{j=1}^2 \prod_{w=1}^m \Gamma(-x_i + \phi_{i,j} + b_{l_{i,j},w}) \prod_{j=1}^2 \prod_{w=1}^n \Gamma(1 + x_i - \phi_{i,j} - a_{l_{i,j},w}) \prod_{j=1}^2 \left(\Gamma(v_{i,j} - x_i) \right)^{k_{i,j}}}{\prod_{j=1}^2 \prod_{w=n+1}^p \Gamma(-x_i + \phi_{i,j} + a_{l_{i,j},w}) \prod_{j=1}^2 \prod_{w=m+1}^q \Gamma(1 + x_i - \phi_{i,j} - b_{l_{i,j},w}) \prod_{j=1}^2 \left(\Gamma(1 + v_{i,j} - x_i) \right)^{k_{i,j}}} \right. \\ & \left. \frac{\Gamma(x_i)}{\Gamma\left(1 + \sum_{i=1}^N x_i\right)} \right] \left(\int_0^\infty e^{-q\gamma} \gamma^{p-1} \gamma^{\frac{1}{t} \sum_{i=1}^N x_i} d\gamma \right) dx_i \end{aligned} \quad (28)$$

We solve the inner integral in (28):

$$\int_0^\infty e^{-q\gamma} \left(\gamma \right)^{p-1 + \frac{1}{t} \sum_{i=1}^N x_i} d\gamma = \left(\frac{1}{q} \right)^{p + \frac{1}{t} \sum_{i=1}^N x_i} \Gamma\left(p + \frac{1}{t} \sum_{i=1}^N x_i \right) \quad (29)$$

Using (29) in (28), we apply the definition of N -multivariate Fox-H function [47, A.1] to get (26). To prove (b), we use the asymptotic analysis in [45, (31)] to express the average BER at a high SNR in (27). To prove (c), we find the diversity order G_{BER} by representing $\bar{P}_e^\infty \propto \gamma_0^{-G_{\text{BER}}}$. ■

Similar to the outage probability, we list the diversity order of RISE-FSO system using the average BER in Table II with $\kappa = 1$.

The average BER of the DL-FSO system can be derived using (11) in (25), and applying the similar procedure used in RISE-FSO with the inner integral $\int_0^\infty e^{-q\gamma} \gamma^{p-1} \gamma^{x/t} d\gamma = \frac{1}{q^{p+\frac{x}{t}}} \Gamma\left(p + \frac{x}{t}\right)$ to get

$$\begin{aligned} \bar{P}_e^{\text{DL}} = & \frac{\psi v^k}{2\Gamma(p)} \sum_{l=1}^P \zeta_l C_l^{-\phi} H_{p+k+2, q+k+1}^{m+k, n+2} \\ & \left[C_l \left(\frac{1}{q\gamma_0} \right)^{1/t} \left| \begin{array}{l} \{(\phi + a_{l,w}, 1)\}_{w=1}^n, (1, 1), (1 - p, \frac{1}{t}), \{(\phi + a_{l,w}, 1)\}_{w=n+1}^p, \{(v + 1, 1)\}_1^k \\ \{(\phi + b_{l,w}, 1)\}_{w=1}^m, \{(v, 1)\}_1^k, \{(\phi + b_{l,w}, 1)\}_{w=m+1}^q, (0, 1) \end{array} \right. \right] \end{aligned} \quad (30)$$

We use the asymptotic analysis of univariate Fox-H function provided in [48] to express average BER of the DL-FSO at a high SNR

$$\bar{P}_e^{\infty, \text{DL}} \approx \frac{\psi v^k}{2\Gamma(p)} \sum_{l=1}^P \zeta_l C_l^{-\phi} \left[\sum_{i=1}^m \frac{\prod_{w=1, w \neq i}^m \Gamma(b_{l,w} - b_{l,i}) (\Gamma(v - \phi - b_{l,i}))^k \prod_{w=1}^n \Gamma(1 - a_{l,w} + b_{l,i}) \Gamma(\phi + b_{l,i}) \Gamma(p + \frac{\phi + b_{l,i}}{t})}{\prod_{w=n+1}^p \Gamma(a_{l,w} - b_{l,i}) (\Gamma(v + 1 - \phi - b_{l,i}))^k \prod_{w=m+1}^q \Gamma(1 - b_{l,w} + b_{l,i}) \Gamma(1 + \phi + b_{l,i})} \right. \\ \left. \left(C_l^{\phi + b_{l,i}} \left(\frac{1}{q\gamma_0} \right)^{(\phi + b_{l,i})/t} \right) + k \frac{\prod_{w=1}^m \Gamma(\phi + b_{l,w} - v) \prod_{w=1}^n \Gamma(1 - \phi - a_{l,w} + v) \Gamma(v) \Gamma(p + \frac{v}{t})}{\prod_{w=n+1}^p \Gamma(\phi + a_{l,w} - v) \prod_{w=m+1}^q \Gamma(1 - \phi - b_{l,w} + v) \Gamma(1 + v)} \left(C_l^v \left(\frac{1}{q\gamma_0} \right)^{v/t} \right) \right] \quad (31)$$

We can express $\bar{P}_e^{\infty, \text{DL}} \propto \gamma_0^{-G_{\text{BER}}^{\text{DL}}}$ to get the BER-diversity order of the DL-FSO system as $G_{\text{BER}}^{\text{DL}} = \min(\{\frac{\phi + b_{l,i}}{t}\}_{l=1, i=1}^{l=P, i=m}, \frac{v}{t})$. Similar to the outage probability, the diversity order of the DL-FSO system for \mathcal{F} , \mathcal{GG} , and \mathcal{M} are given, respectively as $\min\{\frac{\alpha_F}{t}, \frac{\rho^2}{t}, \frac{v}{t}\}$, $\min\{\frac{\rho^2}{t}, \frac{\alpha_G}{t}, \frac{\beta_G}{t}, \frac{v}{t}\}$, and $\min\{\frac{\rho^2}{t}, \frac{\alpha_M}{t}, \frac{\beta_M}{t}, \frac{v}{t}\}$.

C. Ergodic Capacity

Ergodic capacity of an FSO system is given as

$$\bar{\eta} = \mathbb{E}[\log_2(1 + \mu_t \gamma)] = \int_0^\infty \log_2(1 + \mu_t \gamma) f_\gamma(\gamma) d\gamma \quad (32)$$

where $t \in \{1, 2\}$ with $\mu_1 = 1$ HD and $\mu_2 = \frac{\epsilon}{2\pi}$ for the IMM/DD detection.

Lemma 3. *The ergodic capacity of the RISE-FSO is given by*

$$\bar{\eta} = \frac{\log_2(e)}{t} \sum_{l_{1,1}, l_{1,2}=0}^P \cdots \sum_{l_{N,1}, l_{N,2}=0}^P \prod_{i=1}^N \prod_{j=1}^2 \psi_{i,j} v_{i,j}^{k_{i,j}} \zeta_{l_{i,j}} \left(C_{l_{i,j}} \right)^{-\phi_{i,j}} \\ \left[\begin{array}{c} \left(\frac{1}{\epsilon\gamma_0} \right)^{1/t} \prod_{j=1}^2 C_{l_{i,j}} \\ \cdot \\ \cdot \\ \left(\frac{1}{\epsilon\gamma_0} \right)^{1/t} \prod_{j=1}^2 C_{l_{i,j}} \\ \frac{\mu_t}{\epsilon} \end{array} \right] \begin{array}{l} (1, \frac{1}{t}, \dots, \frac{1}{t}, 1) : V_1; (1, 1), (1, 1) \\ (1; 1, \dots, 1, 0) : V_2; (1, 1), (0, 1) \end{array} \quad (3)$$

where $V_1 = \{ \{(\phi_{i,1} + a_{l_{i,1},w}, 1)\}_{w=1}^n, \{(\phi_{i,2} + a_{l_{i,2},w}, 1)\}_{w=1}^n, (1, 1), \{(\phi_{i,1} + a_{l_{i,1},w}, 1)\}_{w=n+1}^p, \{(\phi_{i,2} + a_{l_{i,2},w}, 1)\}_{w=n+1}^p, \{(v_{i,1} + 1, 1)\}_1^{k_{i,1}}, \{(v_{i,2} + 1, 1)\}_1^{k_{i,2}} \}_{i=1}^N$ and $V_2 = \{ \{(\phi_{i,1} + b_{l_{i,1},w}, 1)\}_{w=1}^m, \{(\phi_{i,2} + b_{l_{i,2},w}, 1)\}_{w=1}^m, \{(v_{i,1}, 1)\}_1^{k_{i,1}}, \{(v_{i,2}, 1)\}_1^{k_{i,2}}, \{(\phi_{i,1} + b_{l_{i,1},w}, 1)\}_{w=m+1}^q, \{(\phi_{i,2} + b_{l_{i,2},w}, 1)\}_{w=m+1}^q \}_{i=1}^N$.

Proof:

We substitute the PDF of SNR of RISE-FSO system (20) through (16) in (32), use the definition of multivariate Fox-H function, and change the order of integration to get

$$\bar{\eta} = \frac{\log_2(e)}{t} \sum_{l_{1,1}, l_{1,2}=0}^P \cdots \sum_{l_{N,1}, l_{N,2}=0}^P \prod_{i=1}^N \prod_{j=1}^2 \psi_{i,j} v_{i,j}^{k_{i,j}} \zeta_{l_{i,j}} \left(C_{l_{i,j}} \right)^{-\phi_{i,j}} \left(\left(\frac{1}{2\pi j} \right)^N \int_{\mathcal{L}_i} \left(\left(\frac{1}{\gamma_0} \right)^{1/t} \prod_{j=1}^2 C_{l_{i,j}} \right)^{n_i} \right. \\ \left. \frac{\prod_{j=1}^2 \prod_{w=1}^m \Gamma(-x_i + \phi_{i,j} + b_{l_{i,j},w}) \prod_{j=1}^2 \prod_{w=1}^n \Gamma(1 + x_i - \phi_{i,j} - a_{l_{i,j},w}) \prod_{j=1}^2 \left(\Gamma(v_{i,j} - x_i) \right)^{k_{i,j}}}{\prod_{j=1}^2 \prod_{w=n+1}^p \Gamma(-x_i + \phi_{i,j} + a_{l_{i,j},w}) \prod_{j=1}^2 \prod_{w=m+1}^q \Gamma(1 + x_i - \phi_{i,j} - b_{l_{i,j},w}) \prod_{j=1}^2 \left(\Gamma(1 + v_{i,j} - x_i) \right)^{k_{i,j}}} \right. \\ \left. \frac{\Gamma(x_i)}{\Gamma\left(\sum_{i=1}^N x_i\right)} \right] \left(\int_0^\infty \ln(1 + \mu_t \gamma) \gamma^{-1 + \frac{1}{t} \sum_{i=1}^N x_i} d\gamma \right) dx_i \quad (34)$$

To solve the inner integral in (34), we use [44, 01.04.07.0002.01] to express $\ln(1 + \mu_t \gamma) = \frac{1}{2\pi j} \int_{\mathcal{L}} \frac{\Gamma(u+1)\Gamma(-u)^2}{\Gamma(1-u)} (\mu_t \gamma)^{-u} du$ and use the final value theorem $\lim_{x \rightarrow \infty} \int_0^x f(u) du = \lim_{s \rightarrow 0} F(s) = F(\epsilon)$, where ϵ is close to zero (in the order 10^{-6}). Thus, the inner integral becomes

$$\int_0^\infty \ln(1 + \mu_t \gamma) \left(\gamma \right)^{-1 + \frac{1}{t} \sum_{i=1}^N x_i} d\gamma = \lim_{s \rightarrow 0} \frac{1}{2\pi j} \int_{\mathcal{L}} \frac{\Gamma(u+1)\Gamma(-u)^2}{\Gamma(1-u)} \left(\mu_t \left(\frac{1}{s} \right) \right)^{-u + \frac{1}{t} \sum_{i=1}^N x_i} \Gamma\left(-u + \frac{1}{t} \sum_{i=1}^N x_i\right) du \\ = \frac{1}{2\pi j} \int_{\mathcal{L}} \frac{\Gamma(u+1)\Gamma(-u)^2}{\Gamma(1-u)} \left(\mu_t \left(\frac{1}{\epsilon} \right) \right)^{-u + \frac{1}{t} \sum_{i=1}^N x_i} \Gamma\left(-u + \frac{1}{t} \sum_{i=1}^N x_i\right) du \quad (35)$$

We substitute (35) in (34) and apply the definition of N -multivariate Fox-H function [47, A.1] to get (33). ■

We derive an exact closed form expression of the DL-FSO system by substituting (10) in (32), representing $\ln(1 + \mu_t \gamma)$ in terms of Meijer-G function and applying the identity [44, 07.34.21.0012.01]:

$$\bar{\eta}^{\text{DL}} = \log_2(e) \frac{\psi v^k}{t} \sum_{l=1}^P \zeta_l C_l^{-\phi} H_{p+k+2, q+k+2}^{m+k+2, n+1} \left[C_l \left(\frac{1}{\mu_t \gamma_0} \right)^{1/t} \left| \begin{array}{l} V_1, (0, \frac{1}{t}), (1, \frac{1}{t}), V_2 \\ V_3, (0, \frac{1}{t}), (0, \frac{1}{t}), V_4 \end{array} \right. \right] \quad (36)$$

where $V_1 = \{(\phi + a_{l,w}, 1)\}_{w=1}^n$, $V_2 = \{(\phi + a_{l,w}, 1)\}_{w=n+1}^p, \{(v+1, 1)\}_1^k$, $V_3 = \{(\phi + b_{l,w}, 1)\}_{w=1}^m, \{(v, 1)\}_1^k$ and $V_4 = \{(\phi + b_{l,w}, 1)\}_{w=m+1}^q$.

D. Moments of SNR

Finally, we derive moments of SNR for both RISE-FSO and DL-FSO systems, which can be a useful metric to characterize the average SNR and order of fading.

Lemma 4. *The r -th moment of SNR for the RISE-FSO system is given as*

$$\bar{\gamma}^{(r)} = \mathbb{E}[\gamma^r] = \frac{1}{t} \left(\frac{1}{\epsilon} \right)^r \sum_{l_{1,1}, l_{1,2}=0}^P \cdots \sum_{l_{N,1}, l_{N,2}=0}^P \prod_{i=1}^N \prod_{j=1}^2 \psi_{i,j} v_{i,j}^{k_{i,j}} \zeta_{i,j} \left(C_{l_{i,j}} \right)^{-\phi_{i,j}}$$

$$H_{1,1:2p+k_{1,1}+k_{1,2}, 2n+1; \dots; 2m+k_{N,1}+k_{N,2}, 2n+1}^{0,1:2p+k_{1,1}+k_{1,2}+1, 2q+k_{1,1}+k_{1,2}; \dots; 2p+k_{N,1}+k_{N,2}+1, 2q+k_{N,1}+k_{N,2}} \left[\begin{array}{c} \left(\frac{1}{\epsilon \gamma_0} \right)^{1/t} \prod_{j=1}^2 C_{l_{i,j}} \\ \vdots \\ \left(\frac{1}{\epsilon \gamma_0} \right)^{1/t} \prod_{j=1}^2 C_{l_{i,j}} \end{array} \middle| \begin{array}{l} (1-r, \frac{1}{t}, \dots, \frac{1}{t}) : V_1 \\ (1; 1, \dots, 1) : V_2 \end{array} \right] \quad (37)$$

where $V_1 = \{ \{(\phi_{i,1} + a_{l_{i,1},w}, 1), \{(\phi_{i,2} + a_{l_{i,2},w}, 1)\}_{w=1}^n, (1, 1), \{(\phi_{i,1} + a_{l_{i,1},w}, 1)\}_{w=n+1}^p, \{(\phi_{i,2} + a_{l_{i,2},w}, 1)\}_{w=n+1}^p, \{(v_{i,1} + 1, 1)\}_1^{k_{i,1}}, \{(v_{i,2} + 1, 1)\}_1^{k_{i,2}} \}_{i=1}^N$ and $V_2 = \{ \{(\phi_{i,1} + b_{l_{i,1},w}, 1)\}_{w=1}^m, \{(\phi_{i,2} + b_{l_{i,2},w}, 1)\}_{w=1}^m, \{(v_{i,1}, 1)\}_1^{k_{i,1}}, \{(v_{i,2}, 1)\}_1^{k_{i,2}}, \{(\phi_{i,1} + b_{l_{i,1},w}, 1)\}_{w=m+1}^q, \{(\phi_{i,2} + b_{l_{i,2},w}, 1)\}_{w=m+1}^q \}_{i=1}^N$.

Proof: We substitute the PDF of SNR (20) (using (16)) in $\mathbb{E}[\gamma^r] = \int_0^\infty \gamma^r f_\gamma(\gamma) d\gamma$ to compute the r -th moment of SNR by expanding the definition of Fox's H function:

$$\bar{\gamma}^{(r)} = \frac{1}{t} \sum_{l_{1,1}, l_{1,2}=0}^P \cdots \sum_{l_{N,1}, l_{N,2}=0}^P \prod_{i=1}^N \prod_{j=1}^2 \psi_{i,j} v_{i,j}^{k_{i,j}} \zeta_{i,j} \left(C_{l_{i,j}} \right)^{-\phi_{i,j}} \left(\left(\frac{1}{2\pi j} \right)^N \int_{\mathcal{L}_i} \left(\left(\frac{1}{\gamma_0} \right)^{1/t} \prod_{j=1}^2 C_{l_{i,j}} \right)^{x_i} \right.$$

$$\left[\frac{\prod_{j=1}^2 \prod_{w=1}^m \Gamma(-x_i + \phi_{i,j} + b_{l_{i,j},w}) \prod_{j=1}^2 \prod_{w=1}^n \Gamma(1 + x_i - \phi_{i,j} - a_{l_{i,j},w}) \prod_{j=1}^2 \left(\Gamma(v_{i,j} - x_i) \right)^{k_{i,j}}}{\prod_{j=1}^2 \prod_{w=n+1}^p \Gamma(-x_i + \phi_{i,j} + a_{l_{i,j},w}) \prod_{j=1}^2 \prod_{w=m+1}^q \Gamma(1 + x_i - \phi_{i,j} - b_{l_{i,j},w}) \prod_{j=1}^2 \left(\Gamma(1 + v_{i,j} - x_i) \right)^{k_{i,j}}} \right.$$

$$\left. \frac{\Gamma(x_i)}{\Gamma\left(\sum_{i=1}^N x_i\right)} \right] \left(\int_0^\infty \gamma^r \gamma^{-1 + \frac{1}{t} \sum_{i=1}^N x_i} d\gamma \right) dx_i \quad (38)$$

To solve inner integral in (38) we use the final value theorem:

$$\int_0^\infty \left(\gamma \right)^{r-1 + \frac{1}{t} \sum_{i=1}^N x_i} d\gamma = \left(\frac{1}{\epsilon} \right)^{n + \frac{1}{t} \sum_{i=1}^N x_i} \Gamma\left(r + \frac{1}{t} \sum_{i=1}^N x_i \right) \quad (39)$$

We substitute (39) in (38) and use the definition of N -multivariate Fox-H function [47, A.1] to get (37). \blacksquare

Similarly, we derive an exact closed form expression of the r -th moment of SNR for the DL-FSO system by substituting (10) in $\mathbb{E}[\gamma^r] = \int_0^\infty \gamma^r f_\gamma(\gamma) d\gamma$, expand the Fox's H function, use

the final value theorem to compute the inner integral $\int_0^\infty \gamma^{r-1+\frac{x}{t}} d\gamma = \lim_{s \rightarrow 0} (\frac{1}{s})^{r+\frac{x}{t}} \Gamma(r + \frac{x}{t}) = (\frac{1}{\epsilon})^{r+\frac{x}{t}} \Gamma(r + \frac{x}{t})$ to get:

$$\bar{\gamma}^{(r, \text{DL})} = \mathbb{E}[\gamma^r] = \frac{\psi v^k}{t} \left(\frac{1}{\epsilon}\right)^r \sum_{l=1}^P \zeta_l C_l^{-\phi} H_{p+k+1, q+k}^{m+k, n+1} \left[C_l \left(\frac{1}{\epsilon \gamma_0}\right)^{1/t} \left| \begin{array}{c} (1-r, \frac{1}{t}), \{(\phi + a_{l,w}, 1)\}_{w=1}^n, \{(\phi + a_{l,w}, 1)\}_{w=n+1}^p, \{(v+1, 1)\}_1^k \\ \{(\phi + b_{l,w}, 1)\}_{w=1}^m, \{(v, 1)\}_1^k, \{(\phi + b_{l,w}, 1)\}_{w=m+1}^q \end{array} \right. \right] \quad (40)$$

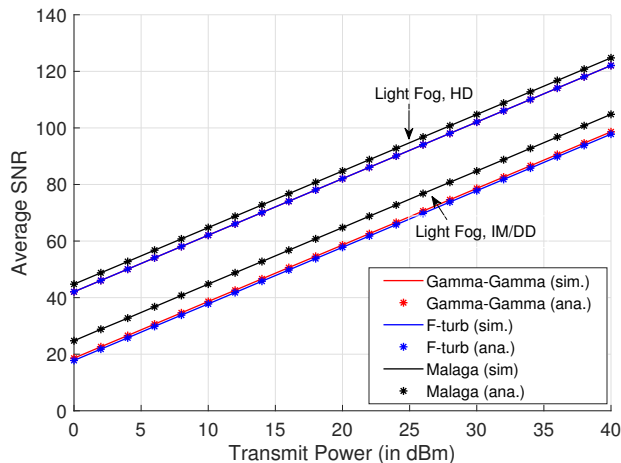
In what follows, we demonstrate the performance of FSO systems using numerical and simulation analysis.

TABLE III
SIMULATION PARAMETERS

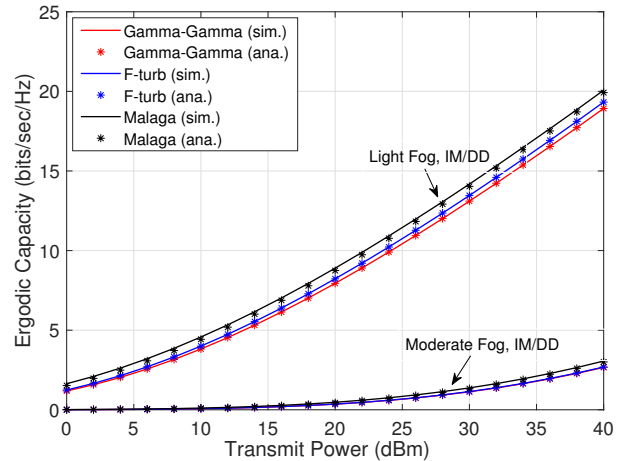
Transmitted power	P_T	0 to 40 dBm
Responsivity	R	0.41 A/W
AWGN variance	σ_v^2	10^{-14} A ² /GHz
Link distance	$\{d, d_1, d_2\}$	{1 km, 500 m, 500 m}
Visibility range	V	{1km, 2km, 3km}
Shape parameter of fog	k	{2.32, 5.49}
Scale parameter of fog	β	{13.12, 12.06}
Aperture diameter	$D = 2a_r$	10 cm
Normalized beam-width	w_z/a_r	15
Normalized jitter	σ_s/a_r	3
Refractive index	C_n^2	$\{5 \times 10^{-14}, 1.25 \times 10^{-14}\}$
Wavelength	λ	1550 nm
\mathcal{F} -distribution	$\{\alpha_F, \beta_F\}$	{4.85, 6.55}, {17.21, 19.24} {17.48, 17.8}, {68.14, 64.73}
$\mathcal{G}\mathcal{G}$ -distribution	$\{\alpha_G, \beta_G\}$	{3.01, 3}, {8.9, 12} {8.17, 11}, {30.76, 40}
\mathcal{M} -distribution	$\{\alpha_M, \beta_M, \Omega, b_0, \rho\}$	{3.01, 3, 1.3265, 0.1079, 0.596}, {8.9, 12, 1.3265, 0.1079, 0.596} {8.17, 11, 1.3265, 0.1079, 0.596}, {30.76, 40, 1.3265, 0.1079, 0.596}

V. SIMULATION AND NUMERICAL RESULTS

In this section, we use numerical analysis and Monte Carlo simulations (averaged over 10^7 channel realizations) to demonstrate the performance of RISE-FSO system under the combined



(a) Average SNR for light fog with HD and IM/DD.



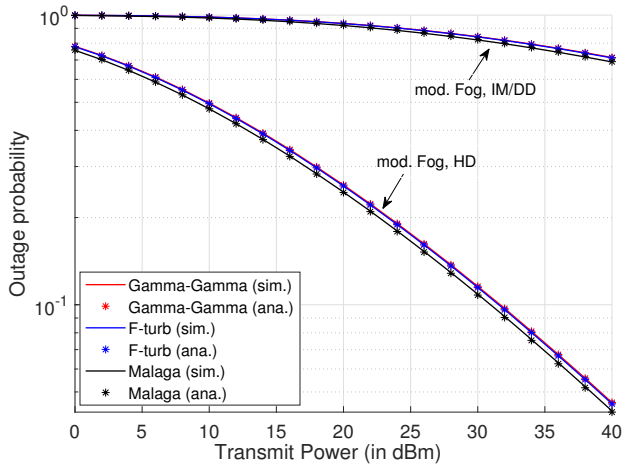
(b) Ergodic capacity for light and moderate fog with IM/DD.

Fig. 1. Average SNR and ergodic capacity of DL-FSO at $d = 1$ km.

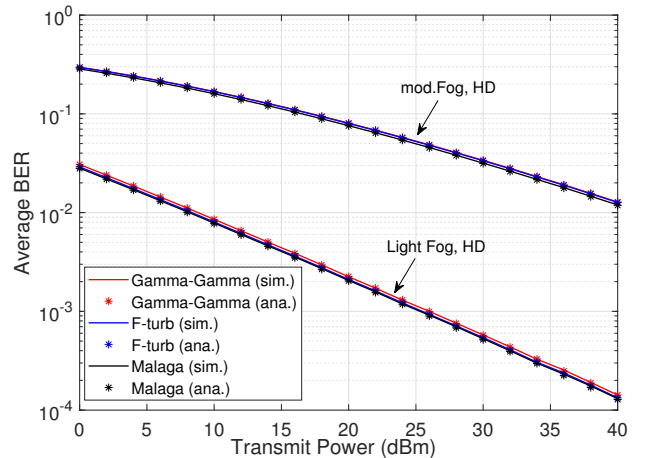
effect of atmospheric turbulence with pointing errors and random fog. We assume a link length of $d = 1$ km and consider that the optical RIS is situated exactly at the mid-way between the source and the destination i.e., $d_1 = d_2 = 500$ m. We study the impact of atmospheric turbulence, pointing errors, and weather conditions on DL-FSO and RISE-FSO systems using both HD and IM/DD detection techniques. We validate our derived analytical expressions through numerical and simulation results. We compute \mathcal{F} -turbulence parameters from [41], $\mathcal{G}\mathcal{G}$ parameters for strong and moderate turbulence from [49], and for the \mathcal{M} distribution, we use $\alpha_M = \alpha_G$ and $\beta_M = \beta_G$. Other simulation parameters are listed in Table III. We also validate our derived analytical expressions through computer simulations. In what follows, we demonstrate the performance of DL-FSO and RISE-FSO systems.

A. DL-FSO system

We demonstrate the performance of a DL-FSO considering a link distance $d = 1$ km under different atmospheric conditions. The impact of fog on the performance of FSO systems for both detection techniques is depicted in Fig. 1 and Fig. 2. In Fig. 1(a), the average SNR performance for the light fog shows that the HD outperforms IM/DD, as expected since the HD detector performs better than the IM/DD for a given atmospheric condition. It can also be seen that the performance of DL-FSO is similar for considered turbulence models. In Fig. 1(b), we compare the performance of IM/DD detector in the presence of light and moderate fog for three turbulence



(a) Outage probability with HD and IM/DD detection for moderate fog and $\gamma_{th} = 5\text{dB}$.



(b) Average BER for light and moderate fog for HD.

Fig. 2. Outage probability and average BER for DL-FSO system at $d = 1\text{km}$.

models. The figure shows that the capacity in the presence of moderate fog is reduced by around 10 times when compared with the light fog scenario at a transmit power of 40dBm.

The outage probability performance of the DL-FSO system over light foggy conditions with HD and IM/DD detection techniques and different turbulence conditions is illustrated in Fig. 2(a). As expected, HD detector outperforms IM/DD even in the presence of moderate fog. Despite the fact that the HD detector performance is relatively better, outage probability is still around 10^{-2} even at $P_t = 40\text{dBm}$. Performance can be significantly improved with the application of RIS, as presented in the next subsection. Fig. 2(b) shows the average BER performance of the DL-FSO system with $p = 0.5$, $q = 1$. The figure shows a significant degradation in the average BER if the fog density increases from light to moderate.

B. RISE-FSO system

To simulate the RISE-FSO system, we calculate turbulence parameters since the distance between source and optical RIS $d_1 = 500\text{m}$ and from RIS to destination $d_2 = 500\text{m}$ is modified. Further, we assume that the effect of atmospheric turbulence, random fog and pointing error impairments are identical for both the hops. For light and moderate foggy conditions, Fig. 3 illustrates the average SNR and capacity of RISE-FSO system versus the number of RIS elements N . The average SNR for both HD and IM/DD detectors in the presence of light fog is plotted in

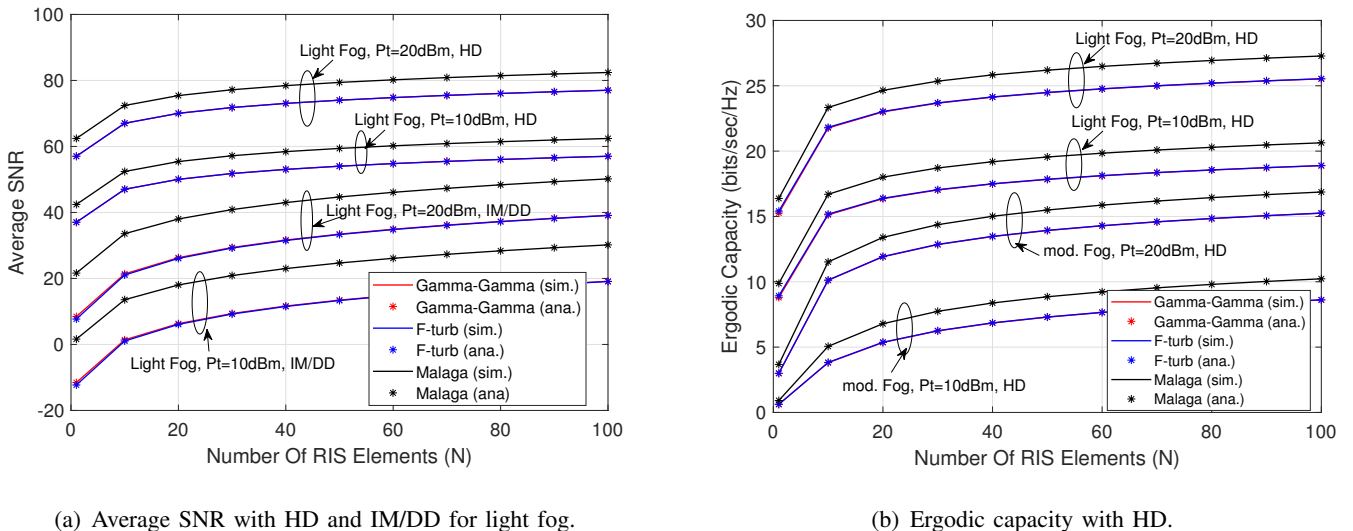


Fig. 3. Average SNR and ergodic capacity of RISE-FSO system at $d_1 = 500\text{m}$, and $d_2 = 500\text{m}$.

Fig. 3(a). We can observe that the HD detector for the RISE-FSO system improves the average SNR performance compared with the IM/DD. Furthermore, the average SNR increases with an increase in the number of RIS elements. Similarly, Fig. 3(b) demonstrates the ergodic capacity when the HD detector is employed in the presence of light and moderate fog conditions. The figure shows that the RIS significantly improves the ergodic capacity performance.

Finally, we demonstrate the outage probability of RISE-FSO system for light and moderate fog conditions with the IM/DD detector in Fig. 4(a). The figure shows that the use of RIS improves the performance of FSO system significantly with a gain of 10dBm of transmit power using $N = 100$ for moderate fog conditions. The impact of RIS elements on the diversity order of RISE-FSO system can also be observed. A key finding is that performance degradation caused by moderate fog can be compensated with a larger N . Thus, an increased number of RIS elements may be required to reduce the impact of atmospheric turbulence and adverse weather conditions. In Fig. 4(b), average BER of the RISE-FSO system (with $p = 0.5$, $q = 1$) is plotted for moderate foggy conditions. It can be seen that the average BER improves significantly with an increase in the number of RIS elements.

VI. CONCLUSIONS

In this paper, we presented exact closed-form expressions on the performance of RIS empowered FSO system under various channel impairments such as atmospheric turbulence, pointing

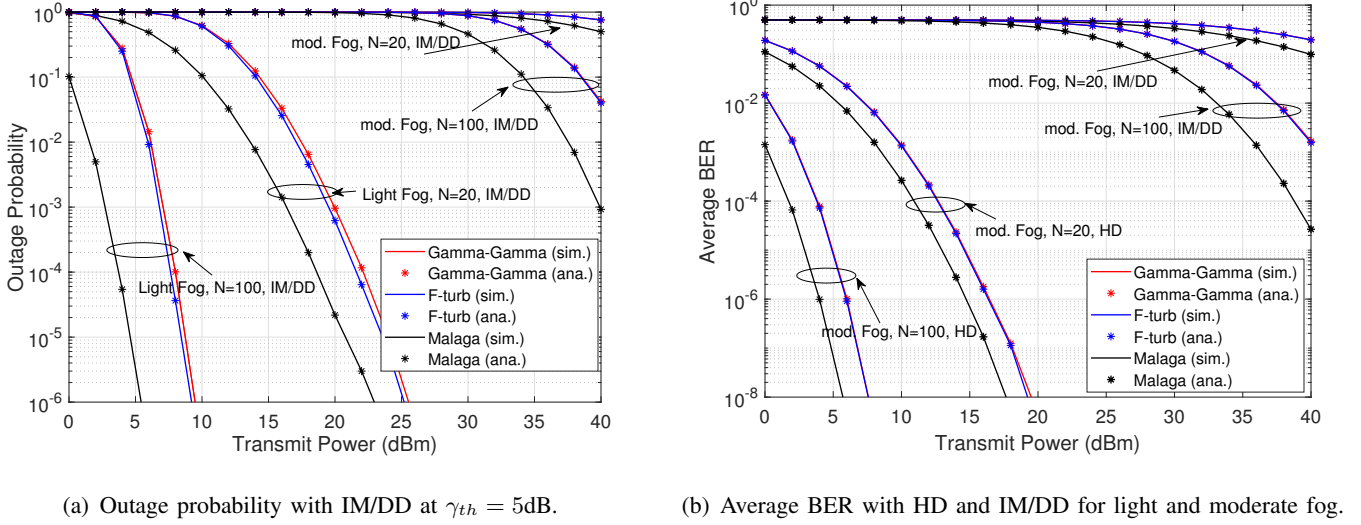


Fig. 4. Outage probability and average BER of RISE-FSO system at $d_1 = 500\text{m}$ and $d_2 = 500\text{m}$.

errors, and different weather conditions. Our derived analytical results are unified allowing evaluation of the RISE-FSO system over \mathcal{F} , \mathcal{GG} , and \mathcal{M} atmospheric turbulence models with pointing errors, deterministic and random path-loss, and considering both HD and IM/DD detection techniques. We developed exact analysis on the performance metrics such as outage probability, average BER, ergodic capacity, and moments of SNR of the RISE-FSO system. Using the asymptotic analysis on the outage probability and average BER, we derived the diversity order providing design aspect of performance enhancement with RIS elements and the mitigation of pointing errors. We provided extensive simulations and numerical analysis to demonstrate the effectiveness of RISE-FSO system comparing with the DL-FSO under various channel conditions. The proposed work demonstrated the application of optical RIS to enhance the performance of FSO system considering a general scenario of atmospheric turbulence, pointing error impairments, weather conditions, and the underlying detection methods. We envision that the RIS technology can empower the deployment of FSO system for next generation wireless networks, especially for terrestrial applications.

APPENDIX A: PDF AND CDF OF DIRECT LINK h_i

Using the joint distribution of conditional random variables, the PDF of $h_i = h_i^{(tp)} h_i^{(f)}$ is given by

$$f_{h_i}(x) = \int_x^\infty \frac{f_{h_i^{(f)}}\left(\frac{x}{u}\right) f_{h_i^{(tp)}}(u)}{u} du \quad (41)$$

Using (7) and (9) in (41), we get

$$f_{h_i}(x) = \psi \frac{v^k}{\Gamma(k)} \sum_{l=1}^P \zeta_l x^{v-1} \int_x^\infty u^{\phi-1} \frac{\ln^{k-1}\left(\frac{u}{x}\right)}{u^v} G_{p,q}^{m,n} \left[C_l u \left| \begin{array}{c} \{a_{l,w}\}_{w=1}^p \\ \{b_{l,w}\}_{w=1}^q \end{array} \right. \right] du \quad (42)$$

We use the definition of Meijer-G function, interchange the order of integration to express (42) as

$$f_{h_i}(x) = \psi \frac{v^k}{\Gamma(k)} \sum_{l=1}^P \zeta_l x^{v-1} \frac{1}{2\pi j} \int_{\mathcal{L}} \frac{\prod_{j=1}^m \Gamma(b_{l,j} - s) \prod_{j=1}^n \Gamma(1 - a_{l,j} + s)}{\prod_{j=n+1}^p \Gamma(a_{l,j} - s) \prod_{j=m+1}^q \Gamma(1 - b_{l,j} + s)} \left(C_l \right)^s \left(\int_x^\infty u^{\phi-v-1} \ln^{k-1}\left(\frac{u}{x}\right) u^s du \right) ds \quad (43)$$

Substituting $\ln\left(\frac{u}{x}\right) = y$ and applying $\frac{1}{v-s-\phi} = \frac{\Gamma(v-s-\phi)}{\Gamma(v-s-\phi+1)}$, the inner integral in (43) can be solved as

$$\int_x^\infty u^{s+\phi-v-1} \ln^{k-1}\left(\frac{u}{x}\right) du = \frac{x^{s+\phi-v} (\Gamma(v-s-\phi+1))^k}{(\Gamma(v-s-\phi))^k} \Gamma(k) \quad (44)$$

Finally, we use (44) in (43) and apply the definition of Meijer's G function, we get (10) of Theorem 1. To derive the CDF, we use the following:

$$F_{h_i}(x) = \int_0^x f_{h_i}(u) du = \psi v^k \sum_{l=1}^P \zeta_l \frac{1}{2\pi j} \int_{\mathcal{L}} \frac{\prod_{j=1}^m \Gamma(b_{l,j} - s) \prod_{j=1}^n \Gamma(1 - a_{l,j} + s)}{\prod_{j=n+1}^p \Gamma(a_{l,j} - s) \prod_{j=m+1}^q \Gamma(1 - b_{l,j} + s)} \frac{\left(\Gamma(v-s-\phi) \right)^k}{\left(\Gamma(v-s-\phi+1) \right)^k} \left(C_l \right)^s \left(\int_0^x v^{s+\phi-1} dv \right) ds \quad (45)$$

Using the solution of inner integral $\int_0^x v^{s+\phi-1} dv = \frac{x^{s+\phi}}{s+\phi} = x^{s+\phi} \frac{\Gamma(s+\phi)}{\Gamma(s+\phi+1)}$ in (45), we apply the definition of Meijer's G function to get (11).

APPENDIX B: PDF, CDF, AND MGF OF Z_i

We use the Mellin transform to derive the PDF of $Z_i = \prod_{j=1}^L h_{i,j}$. Here, $h_{i,j}, j = 1, 2, \dots, L$ are considered to be i.n.i.d random variables distributed according to (10). Thus, the PDF of Z_i is

$$f_{Z_i}(x) = \frac{1}{x} \frac{1}{2\pi j} \int_{\mathcal{L}} \mathbb{E}[Z_i^r] x^{-r} dr \quad (46)$$

where $\mathbb{E}[Z_i^r] = \prod_{j=1}^L \mathbb{E}[h_{i,j}^r] = \prod_{j=1}^L \int_0^\infty u^r f_{h_{i,j}}(u) du$ is the r -th moment of Z_i . We substitute the PDF of $h_{i,j}$ and use the identity [44, 07.34.21.0009.01] to get

$$\begin{aligned}
\int_0^\infty u^r f_{h_{i,j}}(u) du &= \psi_j v_j^{k_j} \sum_{l_j=0}^P \zeta_{l_j} \left(\int_0^\infty u^r u^{\phi_j-1} G_{p+k_j, q+k_j}^{m+k_j, n} \left[C_{l_j} u \left| \begin{array}{l} \{a_{l_j, w}\}_{w=1}^p, \{v - \phi_j + 1\}_1^{k_j} \\ \{b_{l_j, w}\}_{w=1}^m, \{v - \phi_j\}_1^{k_j}, \{b_{l_j, w}\}_{w=m+1}^q \end{array} \right. \right] du \right) \\
&= \psi_j v_j^{k_j} \sum_{l_j=0}^P \zeta_{l_j} \left(C_{l_j} \right)^{-(r+\phi_j)} \left[\frac{\prod_{w=1}^m \Gamma(r + \phi_j + b_{l_j, w}) \prod_{w=1}^n \Gamma(1 - r - \phi_j - a_{l_j, w}) \left(\Gamma(v_j + r) \right)^{k_j}}{\prod_{w=r+1}^p \Gamma(r + \phi_j + a_{l_j, w}) \prod_{w=m+1}^q \Gamma(1 - r - \phi_j - b_{l_j, w}) \left(\Gamma(1 + v_j + r) \right)^{k_j}} \right]
\end{aligned} \tag{47}$$

Thus, the r -th moment of Z_i is given by

$$\begin{aligned}
\mathbb{E}[Z_i^r] &= \sum_{l_1, \dots, l_L=0}^P \prod_{j=1}^L \psi_j v_j^{k_j} \zeta_{l_j} \prod_{j=1}^L \left(C_{l_j} \right)^{-(r+\phi_j)} \\
&\left[\frac{\prod_{j=1}^L \prod_{w=1}^m \Gamma(r + \phi_j + b_{l_j, w}) \prod_{j=1}^L \prod_{w=1}^n \Gamma(1 - r - \phi_j - a_{l_j, w}) \prod_{j=1}^L \left(\Gamma(v_j + r) \right)^{k_j}}{\prod_{j=1}^L \prod_{w=n+1}^p \Gamma(r + \phi_j + a_{l_j, w}) \prod_{j=1}^L \prod_{w=m+1}^q \Gamma(1 - r - \phi_j - b_{l_j, w}) \prod_{j=1}^L \left(\Gamma(1 + v_j + r) \right)^{k_j}} \right]
\end{aligned} \tag{48}$$

We substitute (48) in (46) to get the PDF of Z_i as

$$\begin{aligned}
f_{Z_i}(x) &= \frac{1}{x} \frac{1}{2\pi j} \sum_{l_1, \dots, l_L=0}^P \prod_{j=1}^L \psi_j v_j^{k_j} \zeta_{l_j} \left(C_{l_j} \right)^{-\phi_j} \int_{\mathcal{L}} \left(x \prod_{j=1}^L C_{l_j} \right)^{-r} \\
&\left[\frac{\prod_{j=1}^L \prod_{w=1}^m \Gamma(n + \phi_j + b_{l_j, w}) \prod_{j=1}^L \prod_{w=1}^r \Gamma(1 - r - \phi_j - a_{l_j, w}) \prod_{j=1}^L \left(\Gamma(v_j + r) \right)^{k_j}}{\prod_{j=1}^L \prod_{w=n+1}^p \Gamma(r + \phi_j + a_{l_j, w}) \prod_{j=1}^L \prod_{w=m+1}^q \Gamma(1 - r - \phi_j - b_{l_j, w}) \prod_{j=1}^L \left(\Gamma(1 + v_j + r) \right)^{k_j}} \right] dr
\end{aligned} \tag{49}$$

Finally, we apply the definition of Meijer's G function in (49) to get (13).

The CDF of Z_i can be obtained as $F_{Z_i}(x) = \int_0^x f_{Z_i}(u) du$. Thus,

$$\begin{aligned}
F_{Z_i}(x) &= \frac{1}{2\pi j} \sum_{l_1, \dots, l_L=0}^P \prod_{j=1}^L \psi_j v_j^{k_j} \zeta_{l_j} \left(C_{l_j} \right)^{-\phi_j} \int_{\mathcal{L}} \left(\prod_{j=1}^L C_{l_j} \right)^r \left(\int_0^x u^{r-1} du \right) \\
&\left[\frac{\prod_{j=1}^L \prod_{w=1}^m \Gamma(-r + \phi_j + b_{l_j, w}) \prod_{j=1}^L \prod_{w=1}^n \Gamma(1 + r - \phi_j - a_{l_j, w}) \prod_{j=1}^L \left(\Gamma(v_j - r) \right)^{k_j}}{\prod_{j=1}^L \prod_{w=n+1}^p \Gamma(-r + \phi_j + a_{l_j, w}) \prod_{j=1}^L \prod_{w=m+1}^q \Gamma(1 + r - \phi_j - b_{l_j, w}) \prod_{j=1}^L \left(\Gamma(1 + v_j - r) \right)^{k_j}} \right] dr
\end{aligned} \tag{50}$$

Using the inner integral solved by the identity [[50], (8.331.3)], $\int_0^x u^{r-1} du = (\frac{1}{r})x^r = \frac{\Gamma(r)}{\Gamma(r+1)}x^r$ in (50) and apply the definition of Meijer-G function to get (14).

Similarly, the MGF of Z_i $M_{Z_i}(s) = \mathbb{E}[e^{-sx}] = \int_0^\infty e^{-sx} f_{Z_i}(x) dx$ can be expressed as

$$M_{Z_i}(s) = \frac{1}{2\pi j} \sum_{l_1, \dots, l_L=0}^P \prod_{j=1}^L \psi_j v_j^{k_j} \zeta_{l_j} \left(C_{l_j} \right)^{-\phi_j} \int_{\mathcal{L}} \left(\prod_{j=1}^L C_{l_j} \right)^r \left(\int_0^\infty e^{-sx} x^{r-1} dx \right) \left[\frac{\prod_{j=1}^L \prod_{w=1}^m \Gamma(-r + \phi_j + b_{l_j, w}) \prod_{j=1}^L \prod_{w=1}^n \Gamma(1 + r - \phi_j - a_{l_j, w}) \prod_{j=1}^L \left(\Gamma(v_j - r) \right)^{k_j}}{\prod_{j=1}^L \prod_{w=n+1}^p \Gamma(-r + \phi_j + a_{l_j, w}) \prod_{j=1}^L \prod_{w=m+1}^q \Gamma(1 + r - \phi_j - b_{l_j, w}) \prod_{j=1}^L \left(\Gamma(1 + v_j - r) \right)^{k_j}} \right] dr \quad (51)$$

Substituting the inner integral solution using [[50], (3.381.4)] as $\int_0^\infty e^{-sx} x^{r-1} dx = s^{-r} \Gamma(r)$ in (51), we apply the definition of Meijer-G function to get (15).

APPENDIX C: PDF AND CDF OF Z

We apply the inverse Laplace transform of the MGF to find the PDF of $Z = \sum_{i=1}^N Z_i$ as $f_Z(z) = \mathcal{L}^{-1} \prod_{i=1}^N M_{Z_i}(s)$. Thus, we use (51) and interchange the order of integration to get

$$f_Z(x) = \sum_{l_{1,1}, \dots, l_{1,L}=0}^P \dots \sum_{l_{N,1}, \dots, l_{N,L}=0}^P \prod_{i=1}^N \prod_{j=1}^L \psi_{i,j} v_{i,j}^{k_{i,j}} \zeta_{l_{i,j}} \left(C_{l_{i,j}} \right)^{-\phi_{i,j}} \left(\left(\frac{1}{2\pi j} \right)^N \int_{\mathcal{L}_i} \left(\prod_{j=1}^L C_{l_{i,j}} \right)^{n_i} \left[\frac{\prod_{j=1}^L \prod_{w=1}^m \Gamma(-n_i + \phi_{i,j} + b_{l_{i,j}, w}) \prod_{j=1}^L \prod_{w=1}^n \Gamma(1 + n_i - \phi_{i,j} - a_{l_{i,j}, w}) \prod_{j=1}^L \left(\Gamma(v_{i,j} - n_i) \right)^{k_{i,j}}}{\prod_{j=1}^L \prod_{w=n+1}^p \Gamma(-n_i + \phi_{i,j} + a_{l_{i,j}, w}) \prod_{j=1}^L \prod_{w=m+1}^q \Gamma(1 + n_i - \phi_{i,j} - b_{l_{i,j}, w}) \prod_{j=1}^L \left(\Gamma(1 + v_{i,j} - n_i) \right)^{k_{i,j}}} \right] \Gamma(n_i) \right) \left(\frac{1}{2\pi j} \int_{\mathcal{L}} s^{-\sum_{i=1}^N n_i} e^{sx} ds \right) dn_i \quad (52)$$

To solve the inner integral, we apply [50, 8.315.1]:

$$\int_{\mathcal{L}} s^{\sum_{i=1}^N n_i} e^{sx} ds = \left(\frac{1}{x} \right)^{1 + \sum_{i=1}^N n_i} \frac{2\pi j}{\Gamma(-\sum_{i=1}^N n_i)} \quad (53)$$

Using (53) in (52), and applying the definition of N -Multivariate Fox's H function in [47, A.1], we get (16).

To derive the CDF, we use $F_Z(z) = \mathcal{L}^{-1} \prod_{i=1}^N \frac{M_{Z_i}(s)}{s}$ in (51) to get

$$F_Z(x) = \sum_{l_{1,1}, \dots, l_{1,L}=0}^P \cdots \sum_{l_{N,1}, \dots, l_{N,L}=0}^P \prod_{i=1}^N \prod_{j=1}^L \psi_{i,j} v_{i,j}^{k_{i,j}} \zeta_{l_{i,j}} \left(C_{l_{i,j}} \right)^{-\phi_{i,j}} \left(\left(\frac{1}{2\pi j} \right)^N \int_{\mathcal{L}_i} \left(\prod_{j=1}^L C_{l_{i,j}} \right)^{n_i} \right. \\ \left. \left[\frac{\prod_{j=1}^L \prod_{w=1}^m \Gamma(-n_i + \phi_{i,j} + b_{l_{i,j},w}) \prod_{j=1}^L \prod_{w=1}^n \Gamma(1 + n_i - \phi_{i,j} - a_{l_{i,j},w}) \prod_{j=1}^L \left(\Gamma(v_{i,j} - n_i) \right)^{k_{i,j}}}{\prod_{j=1}^L \prod_{w=n+1}^p \Gamma(-n_i + \phi_{i,j} + a_{l_{i,j},w}) \prod_{j=1}^L \prod_{w=m+1}^q \Gamma(1 + n_i - \phi_{i,j} - b_{l_{i,j},w}) \prod_{j=1}^L \left(\Gamma(1 + v_{i,j} - n_i) \right)^{k_{i,j}}} \right. \right. \\ \left. \left. \Gamma(n_i) \right] \left(\frac{1}{2\pi j} \int_{\mathcal{L}} s^{-1 - \sum_{i=1}^N n_i} e^{sx} ds \right) dn_i \right) \quad (54)$$

We apply [50, 8.315.1] to solve the inner integral in (54):

$$\int_{\mathcal{L}} s^{-1 - \sum_{i=1}^N n_i} e^{sx} ds = \left(\frac{1}{x} \right)^{-\sum_{i=1}^N n_i} \frac{2\pi j}{\Gamma\left(1 + \sum_{i=1}^N n_i\right)} \quad (55)$$

Using (55) in (54), we apply the definition of N -Multivariate Fox's H function in [47, A.1] to get (17) of Theorem 2.

REFERENCES

- [1] M. D. Renzo *et al.*, "Smart radio environments empowered by reconfigurable AI meta-surfaces: An idea whose time has come," *EURASIP J. Wireless Commun. Netw.*, vol. 2019, no. 129, 2019.
- [2] E. Basar *et al.*, "Wireless communications through reconfigurable intelligent surfaces," *IEEE Access*, vol. 7, pp. 116753–116773, 2019.
- [3] M. A. ElMossallamy *et al.*, "Reconfigurable intelligent surfaces for wireless communications: Principles, challenges, and opportunities," *IEEE Trans. Cogn. Commun. Netw.*, vol. 6, no. 3, pp. 990–1002, 2020.
- [4] Q. Wu *et al.*, "Intelligent reflecting surface aided wireless communications: A tutorial," *IEEE Trans. Commun.*, pp. 1–1, 2021.
- [5] X. Yuan *et al.*, "Reconfigurable-intelligent-surface empowered wireless communications: Challenges and opportunities," *IEEE Wireless Communications*, vol. 28, no. 2, pp. 136–143, 2021.
- [6] M. A. Khalighi and M. Uysal, "Survey on free space optical communication: A communication theory perspective," *IEEE Commun. Surveys Tuts.*, vol. 16, no. 4, pp. 2231–2258, Fourthquarter 2014.
- [7] P. Yang *et al.*, "6G wireless communications: Vision and potential techniques," *IEEE Network*, vol. 33, no. 4, pp. 70–75, 2019.
- [8] S. Dang *et al.*, "What should 6G be?" *Nature Electronics*, vol. 3, no. 1, pp. 20–29, 2020.
- [9] M. Safari and M. Uysal, "Relay-assisted free-space optical communication," *IEEE Trans. Wireless Commun.*, vol. 7, no. 12, pp. 5441–5449, 2008.
- [10] I. S. Ansari *et al.*, "Performance analysis of free-space optical links over Málaga (\mathcal{M}) turbulence channels with pointing errors," *IEEE Transactions on Wireless Communications*, vol. 15, no. 1, pp. 91–102, 2016.

- [11] E. Zedini *et al.*, “Dual hop FSO transmission systems over Gamma Gamma turbulence with pointing errors,” *IEEE Trans. Wireless Commun.*, vol. 16, no. 2, pp. 784–796, Feb 2017.
- [12] Y. Zhang *et al.*, “On the performance of dual-hop systems over mixed FSO/mmWave fading channels,” *IEEE Open J. Commun. Soc.*, vol. 1, pp. 477–489, 2020.
- [13] D. Kudathanthirige *et al.*, “Performance analysis of intelligent reflective surfaces for wireless communication,” in *ICC 2020-2020 IEEE Int. Conf. Commun. (ICC)*, 2020, pp. 1–6.
- [14] A. A. A. Boulogeorgos and A. Alexiou, “Ergodic capacity analysis of reconfigurable intelligent surface assisted wireless systems,” in *2020 IEEE 3rd 5G World Forum (5GWF)*, 2020, pp. 395–400.
- [15] A.-A. A. Boulogeorgos and A. Alexiou, “Performance analysis of reconfigurable intelligent surface-assisted wireless systems and comparison with relaying,” *IEEE Access*, vol. 8, pp. 94 463–94 483, 2020.
- [16] L. Yang *et al.*, “Accurate closed-form approximations to channel distributions of RIS-aided wireless systems,” *IEEE Wireless Commun. Lett.*, vol. 9, no. 11, pp. 1985–1989, 2020.
- [17] Q. Tao *et al.*, “Performance analysis of intelligent reflecting surface aided communication systems,” *IEEE Commun. Lett.*, vol. 24, no. 11, pp. 2464–2468, 2020.
- [18] R. C. Ferreira *et al.*, “Bit error probability for large intelligent surfaces under double-Nakagami fading channels,” *IEEE Open J. Commun. Society*, vol. 1, pp. 750–759, 2020.
- [19] D. Selimis *et al.*, “On the performance analysis of RIS-empowered communications over Nakagami-m fading,” *IEEE Commun. Lett.*, pp. 1–1, 2021.
- [20] H. Ibrahim *et al.*, “Exact coverage analysis of intelligent reflecting surfaces with Nakagami-m channels,” *IEEE Trans. Veh. Technol.*, vol. 70, no. 1, pp. 1072–1076, 2021.
- [21] I. Trigui, W. Ajib, and W.-P. Zhu, “A comprehensive study of reconfigurable intelligent surfaces in generalized fading,” [Online], arXiv: 2004.02922, 2020.
- [22] H. Du *et al.*, “Millimeter wave communications with reconfigurable intelligent surfaces: Performance analysis and optimization,” *IEEE Trans. Commun.*, vol. 69, no. 4, pp. 2752–2768, 2021.
- [23] L. Yang *et al.*, “Indoor mixed dual-hop VLC/RF systems through reconfigurable intelligent surfaces,” *IEEE Wireless Commun. Lett.*, vol. 9, no. 11, pp. 1995–1999, 2020.
- [24] L. Yang, W. Guo, and I. S. Ansari, “Mixed dual-hop FSO-RF communication systems through reconfigurable intelligent surface,” *IEEE Commun. Lett.*, vol. 24, no. 7, pp. 1558–1562, 2020.
- [25] A. Sikri *et al.*, “Reconfigurable intelligent surface for mixed FSO-RF systems with co-channel interference,” *IEEE Communications Letters*, vol. 25, no. 5, pp. 1605–1609, 2021.
- [26] V. Jamali *et al.*, “Intelligent reflecting surface-assisted free-space optical communications,” arXiv:2105.13297, 2021.
- [27] M. Najafi and R. Schober, “Intelligent reflecting surfaces for free space optical communications,” in *2019 IEEE Global Communications Conference (GLOBECOM)*, 2019, pp. 1–7.
- [28] H. Wang *et al.*, “Performance of wireless optical communication with reconfigurable intelligent surfaces and random obstacles,” arXiv:2001.05715, 2020.
- [29] L. Yang *et al.*, “Free-space optical communication with reconfigurable intelligent surfaces,” ArXiv: 2012.00547, 2020.
- [30] A. R. Ndjiongue *et al.*, “Performance analysis of RIS-based nT-FSO link over \mathcal{G} - \mathcal{G} turbulence with pointing errors,” arXiv: 2102.03654, 2021.
- [31] M. Al-Habash *et al.*, “Mathematical model for the irradiance PDF of a laser beam propagating through turbulent media,” *Opt. Eng.*, vol. 40, pp. 1554–1562, 08 2001.
- [32] A. Jurado-Navas *et al.*, “A unifying statistical model for atmospheric optical scintillation,” *Numerical Simulations of Physical and Engineering Processes*, Sep 2011.

- [33] K. P. Peppas *et al.*, “The fisher–snedecor \mathcal{F} -distribution model for turbulence-induced fading in free-space optical systems,” *J. Lightw. Technol.*, vol. 38, no. 6, pp. 1286–1295, 2020.
- [34] A. A. Farid and S. Hranilovic, “Outage capacity optimization for free-space optical links with pointing errors,” *J. Lightw. Technol.*, vol. 25, no. 7, pp. 1702–1710, July 2007.
- [35] I. I. Kim *et al.*, “Comparison of laser beam propagation at 785 nm and 1550 nm in fog and haze for optical wireless communications,” *Proc. SPIE*, vol. 4214, pp. 26–37, Nov. 2001.
- [36] M. A. Esmail *et al.*, “On the performance of optical wireless links over random foggy channels,” *IEEE Access*, vol. 5, pp. 2894–2903, 2017.
- [37] L. Kong *et al.*, “Effective rate evaluation of RIS-assisted communications using the sums of cascaded α - μ random variates,” *IEEE Access*, vol. 9, pp. 5832–5844, 2021.
- [38] H. Du *et al.*, “Reconfigurable intelligent surface aided TeraHertz communications under misalignment and hardware impairments,” [Online] arXiv: 2012.00267, 2020.
- [39] A. Al-Habash *et al.*, “Mathematical model for the irradiance probability density function of a laser beam propagating through turbulent media,” *Optical Engineering*, vol. 40, no. 8, pp. 1554 – 1562, 2001.
- [40] H. G. Sandalidis *et al.*, “BER performance of FSO links over strong atmospheric turbulence channels with pointing errors,” *IEEE Communications Letters*, vol. 12, no. 1, pp. 44–46, 2008.
- [41] O. Badarneh *et al.*, “Performance analysis of FSO communications over (\mathcal{F}) turbulence channels with pointing errors,” *IEEE Communications Letters*, vol. PP, pp. 1–5, 12 2020.
- [42] Z. Rahman *et al.*, “Performance of opportunistic receiver beam selection in multiaperture OWC systems over foggy channels,” *IEEE Syst. J.*, vol. 14, no. 3, pp. 4036–4046, 2020.
- [43] Z. Rahman *et al.*, “Performance of dual-hop relaying for OWC system over foggy channel with pointing errors and atmospheric turbulence,” arXiv 2105.14256: 2021.
- [44] *The Wolfram function Site*, Available: <https://functions.wolfram.com/>.
- [45] Y. Abo Rahama *et al.*, “On the sum of independent Fox’s H -function variates with applications,” *IEEE Trans. Vehi. Technol.*, vol. 67, no. 8, pp. 6752–6760, 2018.
- [46] I. S. Ansari *et al.*, “A new formula for the BER of binary modulations with dual-branch selection over generalized-K composite fading channels,” *IEEE Transactions on Communications*, vol. 59, no. 10, pp. 2654–2658, 2011.
- [47] A. Mathai *et al.*, *The H-Function: Theory and Applications*.
- [48] H. R. Alhennawi *et al.*, “Closed-form exact and asymptotic expressions for the symbol error rate and capacity of the H -function fading channel,” *IEEE Transactions on Vehicular Technology*, vol. 65, no. 4, pp. 1957–1974, 2016.
- [49] W. Gappmair, “Further results on the capacity of free-space optical channels in turbulent atmosphere,” *Communications, IET*, vol. 5, p. 1262 – 1267, 07 2011.
- [50] I. Gradshteuin *et al.*, *Table of Integrals, Series, And Products*, 01 2007.